

Value-Penalized Auxiliary Control from Examples for Learning without Rewards or Demonstrations

Trevor Ablett¹, Bryan Chan², Jayce Haoran Wang¹, Jonathan Kelly¹

¹University of Toronto, ²University of Alberta

Abstract: Learning from examples of success is an appealing approach to reinforcement learning that eliminates many of the disadvantages of using hand-crafted reward functions or full expert-demonstration trajectories, both of which can be difficult to acquire, biased, or suboptimal. However, learning from examples alone dramatically increases the exploration challenge, especially for complex tasks. This work introduces value-penalized auxiliary control from examples (VPACE); we significantly improve exploration in example-based control by adding scheduled auxiliary control and examples of auxiliary tasks. Furthermore, we identify a value-calibration problem, where policy value estimates can exceed their theoretical limits based on successful data. We resolve this problem, which is exacerbated by learning auxiliary tasks, through the addition of an above-success-level value penalty. Across three simulated and one real robotic manipulation environment, and 21 different main tasks, we show that our approach substantially improves learning efficiency. Videos, code, and datasets are available at <https://papers.starslab.ca/vpace>.

Keywords: Inverse Reinforcement Learning, Multitask Learning, Manipulation

1 Introduction

Robotics presents a unique challenge to learning algorithms: feedback is often formulated as a manually-defined *dense* reward function, or demonstration trajectories of an expert completing the task, both of which can be difficult to acquire, suboptimal, or biased. Ensuring that expert trajectories are nearly optimal, or, alternatively, learning an optimal policy from mixed or suboptimal data, are both challenging, open problems in imitation learning [1]. *Sparse* reward functions are less biased [2], but require significant exploration and can be non-trivial to acquire.

We consider another form of feedback—*example states* of completed tasks. Obtaining example states can be far less laborious than designing a reward function or gathering trajectories: practitioners can gather states from a distribution that represents a completed task without consideration of *how* the states are reached by the expert. Learning from example states, equivalently referred to as example-based control [3], can be inefficient, however. Similar to sparse rewards, the example states provide no information about which actions led to the goal state(s). In robotics applications, this inefficiency is particularly undesirable, since executing suboptimal policies is costly both in terms of potentially destructive environmental effects and time. In this work, we aim to address the following question:

Is it possible to learn policies efficiently given only example states of completed tasks?

To answer this question, we propose a new example-based control method, **value-penalized auxiliary control from examples (VPACE)**. Our approach is inspired by LfGP [4], a method that introduces the use of a scheduler and expert trajectories of *auxiliary* tasks to improve exploration. We build upon this idea to leverage only example states rather than expert trajectories. Our contributions are fourfold: (i) We find that the naïve application of scheduled auxiliary tasks to example-

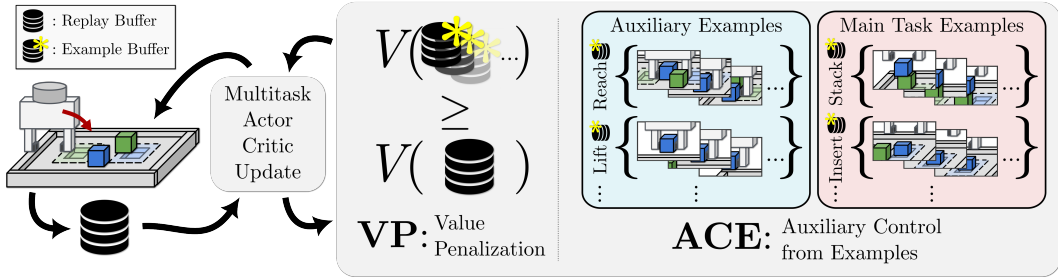


Figure 1: VPACE in a standard reinforcement learning loop and multitask actor-critic update. Value penalization ensures that all example state buffers have higher value than all other states, while auxiliary control from examples allows us to learn from auxiliary task examples instead of main tasks alone.

based control can result in poorly-calibrated value estimates, and we alleviate this problem by introducing value penalization based on the current expected value of the provided examples. The combination and complimentary nature of these two additions results in a dramatic improvement in sample efficiency and performance across four environments with 19 simulated and two real tasks (see Fig. 2) compared with prior state-of-the-art example-based control (RCE, [3]) and imitation learning (DAC, [5], SQIL [6]) approaches. (ii) We situate our approach among these baselines, showing the effects of mixing value penalization and auxiliary control under various reward-modelling assumptions. (iii) We demonstrate that VPACE can be as sample-efficient as learning algorithms with other forms of feedback including expert trajectories and reward functions. (iv) Finally, we theoretically show that our value-penalized objective does not prevent an agent from learning the optimal policy.

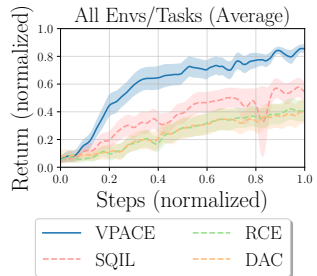


Figure 2: Average normalized results for all tasks studied in this work.

2 Related Work

Sparse rewards are a desirable form of feedback for learning unbiased, optimal policies in reinforcement learning (RL), but they can be difficult to obtain, and present an immense exploration challenge on long-horizon tasks [7]. Reward shaping [8] and dense rewards can help alleviate the exploration problem in robotics [9, 10, 11], but designing dense rewards is difficult for practitioners [12], and can lead to surprising, biased, and suboptimal policies. An alternative to manually-defined rewards is to perform inverse RL (IRL), in which a reward function is recovered from demonstrations, and a policy is learned either subsequently [13, 14, 15] or simultaneously, in a process known as adversarial imitation learning (AIL) [5, 6, 16, 17, 18]. AIL actor-critic approaches can be further divided into methods that learn both a value function and a separate reward model [16, 17] or methods that learn a value function only [5, 6, 18].

Like dense rewards, full trajectory demonstrations can be hard to acquire, suboptimal, or biased. Unlike IRL/AIL, in *example-based control* (EBC), a learning agent is only provided distributions of single *successful example states*. Previous EBC approaches include using generative AIL (GAIL, [16]) directly (VICE, [19]), soft actor critic (SAC, [20]) with an additional mechanism for generating extra success examples (VICE-RAQ, [21]), learning the goal distribution as a reward function (DisCo RL, [22]), performing offline RL with conservative Q learning (CQL, [23]) and a learned reward function [24], and using SAC with a classifier-based reward (RCE, [3]).

All EBC methods can naturally suffer from poor exploration, given that success examples are akin to sparse rewards. Hierarchical reinforcement learning (HRL) aims to leverage multiple levels of abstraction in long-horizon tasks [25], improving exploration in RL both theoretically [26, 27, 28] and empirically [29, 30]. Scheduled auxiliary control (SAC-X, [31]) combines a scheduler with semantically meaningful and simple auxiliary sparse rewards. SAC-X has also been extended to the domain of imitation learning with full trajectories (LfGP, [4, 32, 33]). Our approach builds on

aspects of VICE-RAQ [21], SQIL [6], RCE [3], and LfGP [4], in that we use off-policy learning without a separate reward model to maximize efficiency.

3 Example-Based Control with Value-Penalization and Auxiliary Tasks

Our goal is to generate an agent, with as few environment interactions as possible, that can complete a task given *final state examples* of both the successfully completed task and a small set of reusable auxiliary tasks, with no known reward function or full-trajectory demonstrations. We begin by formally describing the problem setting for example-based control in Section 3.1. In Section 3.2, we describe how scheduled auxiliary tasks can be applied to example-based control. Finally, motivated by the increased exploration diversity of the multitask framework, we propose a new Q-estimation objective in Section 3.3 that leverages value penalization for improved learning stability.

3.1 Problem Setting

A Markov decision process (MDP) is defined as $\mathcal{M} = \langle \mathcal{S}, \mathcal{A}, R, \mathcal{P}, \rho_0, \gamma \rangle$, where the sets \mathcal{S} and \mathcal{A} are respectively the state and action space, \mathcal{P} is the state-transition environment dynamics distribution, ρ_0 is the initial state distribution, γ is the discount factor, and the true reward $R : \mathcal{S} \times \mathcal{A} \rightarrow \mathbb{R}$ is unknown. Actions are sampled from a stochastic policy $\pi(a|s)$. The policy π interacts with the environment to yield experience (s_t, a_t, s_{t+1}) , generated by $s_0 \sim \rho_0(\cdot)$, $a \sim \pi(\cdot|s_t)$, and $s_{t+1} \sim \mathcal{P}(\cdot|s_t, a_t)$. The gathered experience (s_t, a_t, s_{t+1}) is then stored in a buffer \mathcal{B} , which may be used throughout learning. When referring to finite-horizon tasks, $t = T$ indicates the final timestep of a trajectory. For any variables x_t, x_{t+1} , we may drop the subscripts and use x, x' instead when the context is clear.

In this work, we focus on *example-based control*, a more difficult form of imitation learning where we are only given a finite set of example states $s^* \in \mathcal{B}^*$, where $\mathcal{B}^* \subseteq \mathcal{S}$ and $|\mathcal{B}^*| < \infty$, representing a completed task. The goal is to (i) leverage \mathcal{B}^* and \mathcal{B} to learn or define a state-conditional reward function $\hat{R} : \mathcal{S} \rightarrow \mathbb{R}$ that satisfies $\hat{R}(s^*) \geq \hat{R}(s)$ for all $(s^*, s) \in \mathcal{B}^* \times \mathcal{B}$, and (ii) learn a policy $\hat{\pi}$ that maximizes the expected return $\hat{\pi} = \arg \max_{\pi} \mathbb{E}_{\pi} \left[\sum_{t=0}^{\infty} \gamma^t \hat{R}(s_t) \right]$. For any policy π , we can define the value function and Q-function respectively to be:

$$V^{\pi}(s) = \mathbb{E}_{a \sim \pi} [Q^{\pi}(s, a)], \quad (1) \quad Q^{\pi}(s, a) = \hat{R}(s) + \gamma \mathbb{E}_{s' \sim \mathcal{P}} [V^{\pi}(s')], \quad (2)$$

corresponding to the return-to-go from state s (and action a). Both the value function and the Q-function for any policy π satisfy the above Bellman equations that can be used for reinforcement learning (RL), specifically by temporal difference (TD) algorithms.

One way to learn the reward function is through adversarial imitation learning (AIL)—the learned reward function \hat{R} is derived from the minimax objective [5, 16, 17]:

$$\mathcal{L}(D) = \mathbb{E}_{s \sim \mathcal{B}} [\log(1 - D(s))] + \mathbb{E}_{s^* \sim \mathcal{B}^*} [\log(D(s^*))], \quad (3)$$

where D attempts to differentiate the occupancy measure between the state distributions induced by \mathcal{B}^* and \mathcal{B} . The output of $D(s)$ is used to define $\hat{R}(s)$, which is then used for updating the Q-function with Eq. (2). In the single-task regime, this is algorithmically identical to state-only AIL approaches with full demonstrations [34, 35].

3.2 Learning a Multitask Agent from Examples

Example-based control presents a challenging exploration problem for complex tasks. We alleviate this problem by adapting learning from guided play (LfGP) [4], an approach for improving exploration by learning from auxiliary-task expert data, in addition to main task data. Auxiliary tasks are selected to have semantic meaning (e.g. reach, lift). Individual task definitions, and sometimes the auxiliary example data themselves, are reusable between main tasks.

LfGP augments an MDP \mathcal{M} to contain auxiliary tasks, where $\mathcal{T}_{\text{aux}} = \{\mathcal{T}_1, \dots, \mathcal{T}_K\}$ are separate MDPs that share $\mathcal{S}, \mathcal{A}, \mathcal{P}, \rho_0$ and γ with the main task $\mathcal{T}_{\text{main}}$. Each task $\mathcal{T} \in \mathcal{T}_{\text{all}}$ has an example state buffer $\mathcal{B}_{\mathcal{T}}^*$, where $\mathcal{T}_{\text{all}} = \mathcal{T}_{\text{aux}} \cup \{\mathcal{T}_{\text{main}}\}$ is the set of all tasks and we refer to all task-specific entities in our model as $(\cdot)_{\mathcal{T}}$.

The agent consists of multiple components for each task \mathcal{T} , specifically $Q_{\mathcal{T}}, \pi_{\mathcal{T}}$, and optionally $D_{\mathcal{T}}$. Each $\pi_{\mathcal{T}}$ maximizes the joint policy objective

$$\mathcal{L}(\pi) = \sum_{\mathcal{T} \in \mathcal{T}_{\text{all}}} \mathbb{E}_{s \sim \mathcal{B}_{\text{all}}, a \sim \pi_{\mathcal{T}}(\cdot|s)} [Q_{\mathcal{T}}(s, a)], \quad (4)$$

and each $Q_{\mathcal{T}}$ minimizes the joint Bellman residual

$$\mathcal{L}(Q) = \sum_{\mathcal{T} \in \mathcal{T}_{\text{all}}} \mathbb{E}_{(s, \cdot, s') \sim \mathcal{B}} [(Q_{\mathcal{T}} - y_{\mathcal{T}}(s, s'))^2] + \mathbb{E}_{s^* \sim \mathcal{B}_{\mathcal{T}}^*} [(Q_{\mathcal{T}} - y_{\mathcal{T}}(s^*, s^*))^2], \quad (5)$$

where $y_{\mathcal{T}}$ are TD targets defined based on Eq. (2) with task-specific reward $\hat{R}_{\mathcal{T}}$.

Finally, a scheduler selects $\pi_{\mathcal{T}}$ to sample actions from during each environment interaction. Following [4, 31], the scheduler has a fixed period, allowing for a set number of policy switches in each episode. We use a weighted random scheduler and a small set of simple handcrafted high-level trajectories (e.g., *reach* then *lift*), following results from [4], where this approach performed as well as a more complex learned scheduler. The probability of choosing the main task is a hyperparameter $p_{\mathcal{T}_{\text{main}}}$, and each auxiliary task is chosen with probability $p_{\mathcal{T}_k} = (1 - p_{\mathcal{T}_{\text{main}}})/K$. See Appendix D.6.2 for more scheduler details, including the full set of high-level trajectories.

3.3 Value Penalization in Example-Based Control

A scheduled multitask agent will, by design, exhibit far more diverse behaviour than a single-task policy [4, 31]. We show in Section 4.2 that the buffer generated by this behavior, consisting of transitions resulting from multiple policies $\pi_{\mathcal{T}}$, can result in highly unstable and poorly calibrated Q estimates, especially in example-based control. In this section, we extend TD-error minimization, a fundamental component of many off-policy RL algorithms, with a penalty that encourages Q-function outputs to stay well-calibrated with respect to the reward model. Generally, the choice of the reward model and the loss function for estimating the Q-function can greatly impact learning efficiency (see Appendices A and B for details), but our value-penalty term applies to any reward model and commonly used regression-based loss functions. This penalty applies to both the single-task and multitask regime. For simplicity, we describe value penalization for the single-task framework.

Consider a reward model $\hat{R}(\cdot)$ where $\hat{R}(s^*), s^* \in \mathcal{B}^*$, indicates reward for successful states, while $\hat{R}(s), s \in \mathcal{B}$, for all other states. In AIL, \hat{R} is a function of D , while in SQIL [6], for example, $\hat{R}(s^*) = 1$ and $\hat{R}(s) = 0$. Assuming that s^* transitions to itself, then for policy evaluation with the mean-squared error (MSE), we can write the TD target, $y : \mathcal{S} \times \mathcal{S} \rightarrow \mathbb{R}$, of Q-updates as

$$y(s, s') = \hat{R}(s) + \gamma \mathbb{E}_{a'} [Q(s', a')], \quad (6) \quad y(s^*, s^*) = \hat{R}(s^*) + \gamma \mathbb{E}_{a'} [Q(s^*, a')], \quad (7)$$

where $(s, \cdot, s') \sim \mathcal{B}$, $a' \sim \pi(\cdot|s')$, and $s^* \sim \mathcal{B}^*$. Eq. (7) can be replaced with $y(s^*, s^*) = \hat{R}(s^*)$ if one considers successful states to be terminal, but this can cause bootstrapping errors when a task times out or does not terminate upon success [36], both of which are common practice in robotics environments. Regressing to TD targets Eqs. (6) and (7) will eventually satisfy the Bellman equation, but in the short term the targets do not satisfy $y(s, s') \leq y(s^*, s^*)$. This is because the TD targets leverage bootstrapping of the current Q-estimate, an estimate that may not satisfy the Bellman equation and can exceed the bounds of valid Q-values, implying that approximation error of Q updated with the MSE can be uncontrollable.

We introduce a simple resolution to this issue by adding a penalty to our TD updates for $s \in \mathcal{B}$ based on the current estimate of $\mathbb{E}_{s^* \sim \mathcal{B}^*} [V^{\pi}(s^*)]$. This penalty term enforces the Q-estimate to focus on outputting valid values and drives the TD targets to satisfy the inequality $y(s, s') \leq y(s^*, s^*)$. We introduce both a minimum and maximum value for $Q^{\pi}(s, a)$ respectively as

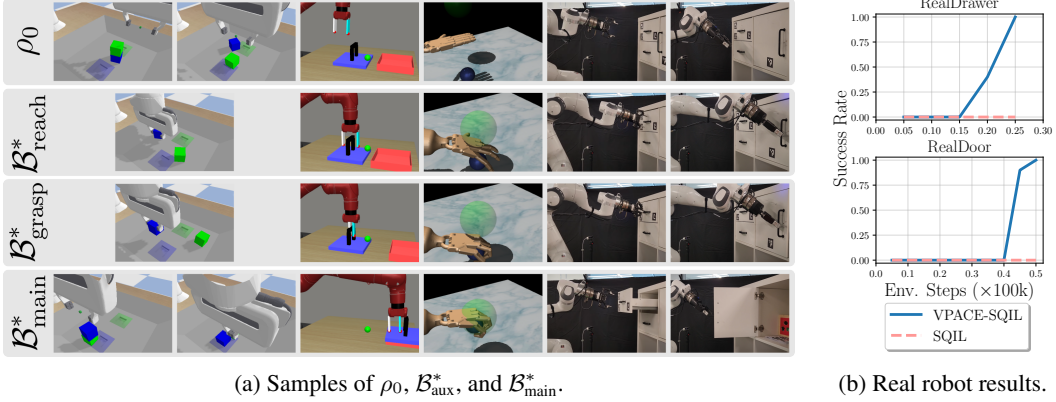


Figure 3: **Left:** Examples from the initial state distribution ρ_0 , auxiliary task example buffers $\mathcal{B}_{\text{aux}}^*$, and main task example buffers $\mathcal{B}_{\text{main}}^*$ for Unstack-Stack, Insert, sawyer_box_close, relocate-human-v0(-dp), RealDrawer, and RealDoor (see Appendix D.4 for all tasks). **Right:** Performance results for our two real robotic tasks.

$$Q_{\min}^{\pi} = \hat{R}_{\min} / (1 - \gamma), \quad (8) \quad Q_{\max}^{\pi} = \mathbb{E}_{s^* \sim \mathcal{B}^*} [V^{\pi}(s^*)], \quad (9)$$

where $\hat{R}_{\min} \leq \hat{R}(s)$ for all $s \in \mathcal{B}$. Then, the value penalty is

$$\mathcal{L}_{\text{pen}}^{\pi}(Q) = \lambda \mathbb{E}_{(s,a) \sim \mathcal{B}} \left[(\max(Q(s,a) - Q_{\max}^{\pi}, 0))^2 + (\max(Q_{\min}^{\pi} - Q(s,a), 0))^2 \right], \quad (10)$$

where $\lambda \geq 0$ is a hyperparameter. Notice that when $\lambda \rightarrow \infty$, Eq. (10) becomes a hard constraint that is only satisfied by functions with valid outputs. It immediately follows that $y(s, s') \leq y(s^*, s^*)$ holds with TD updates Eqs. (6) and (7).

We add value penalization $\mathcal{L}_{\text{pen}}^{\pi}(Q)$ to the MSE loss as a regularization term for learning the Q -function. In Appendix C, we show that the optimal solution of this regularized loss achieves low error on the unregularized loss. Consequently, if we use the regularized loss in policy evaluation, approximate policy iteration (API) still converges to the optimal solution. We state here the informal result that bounds the value error (see Theorem 1 in Appendix C for the formal theorem):

Informal Theorem. *Suppose the function class \mathcal{Q} has bounded output and contains Q^{π} for all π , and suppose we use the value-penalization loss for policy evaluation in API with N samples for each iteration. Then, after k iterations of API, we have that with probability at least $1 - \delta$,*

$$\|Q^* - Q^{\pi_k}\|_{2, \rho_0} \leq \tilde{O} \left(\frac{1}{(1 - \gamma)} \sqrt{\frac{\log(k/\delta)}{2N}} \right),$$

where \tilde{O} hides the constants and concentrability coefficients.

4 Experiments

Through our experiments, we seek to understand if VPACE improves stability and efficiency in example-based control. We also complete an ablation study of various hyperparameter options, and finally analyze the learned values for agents with and without value penalization.

4.1 Experimental Setup

We learn agents in a large variety of tasks and environments, including those originally used in LfGP [4] and RCE [3]. Specifically, the tasks from [4] involve a simulated Franka Emika Panda manipulator, a blue and green block, a fixed “bring” area for each block, and a small slot with < 1 mm tolerance for inserting each block. The environment has a single, shared observation space and action space with multiple options for main and auxiliary tasks. We additionally study all tasks

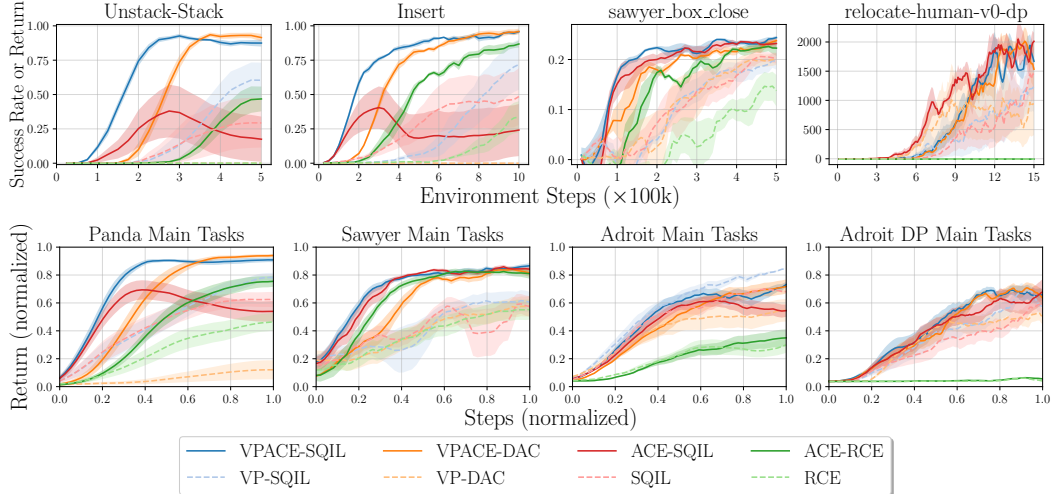


Figure 4: **Top row:** Performance results for four of the most challenging main tasks we considered. **Bottom row:** Average normalized performance for all main tasks we considered, separated by environment. A more detailed task performance breakdown can be found in Appendix E. Performance on auxiliary tasks is not shown. Methods that leverage ACE are shown with solid lines, and their single-task counterparts are shown with dashed lines. The shaded area corresponds to half standard deviation across five seeds (top), or a quarter standard deviation across tasks (bottom). To improve clarity, performance at each step is presented as an average across the five closest timesteps. Both value-penalization and auxiliary task exploration are beneficial for the most complicated tasks.

from [3]: a slightly modified subset of those from [11], involving a simulated Sawyer arm, and three of the Adroit hand tasks originally presented in [37]. We also generate three modified Adroit hand environments that use delta-position action spaces, instead of the absolute positions from the original environments, because we have found that policies learned in the original environments are very coarse and exploit simulator bugs (see Appendix D.2 for details). Finally, we study drawer and door opening tasks with a real Franka Emika Panda.

The reward models that we consider are a learned discriminator (Eq. (3), [5]), SQIL (Eq. (11) and Eq. (12), [6]), and RCE (Eq. (13) and Eq. (14), [3]). For each of these reward models, we can include value penalization (*VP*), auxiliary control from examples (*ACE*), or both (*VPACE*). *VPACE-RCE* and *VP-RCE* are not considered because RCE circumvents the issue of value penalization through its classification-based approach to updating value functions (see Appendix A.3).

All *VPACE* and *ACE* algorithms learn from examples of completed auxiliary tasks, in addition to the main task. In the simulated Panda environment, all main tasks use *release*, *reach*, *grasp*, and *lift* as auxiliary tasks, and each auxiliary task example dataset is reused between main tasks. In the Sawyer, Adroit, and real Panda environments, each main task uses *reach* and *grasp* as auxiliary tasks. Our scheduler approach for all environments is the same weighted random scheduler with a small set of handcrafted trajectories from [4]. All implementations are built on soft actor-critic (SAC) [20]. For more environment, algorithm, task, and implementation details, see Appendix D.

4.2 Main Task Performance Results

Our results for all algorithms for four of the most challenging *main* tasks we examined are shown at the top of Fig. 4, while the bottom shows normalized average results for all tasks, separated by environment. Our real Panda results are shown in Fig. 3b. Since the Sawyer and Adroit tasks do not include specific success evaluation metrics, we only report returns. Policies are evaluated at 25k (environment step) intervals for 50 episodes for the simulated Panda tasks, 10k intervals for 30 episodes for the Sawyer and Adroit tasks, and 5k intervals for 10 episodes for the real Panda tasks.

Our results clearly show the benefits of combining auxiliary task exploration with value penalization. For most tasks, *VPACE-SQIL* learns faster and more stably than any other method. Notably,

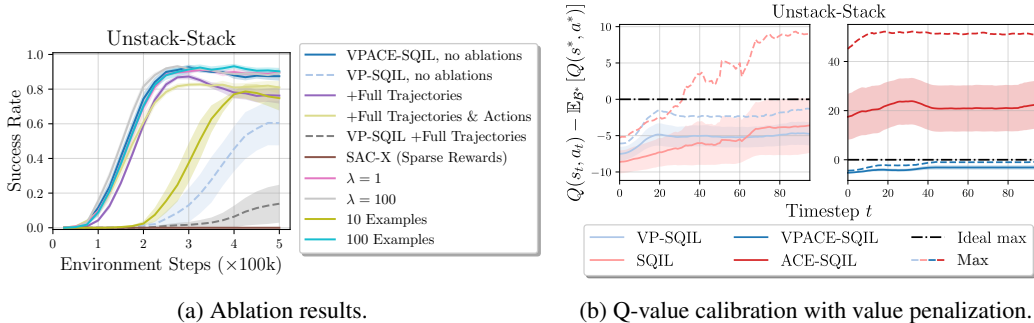


Figure 5: **Left:** Results for changes in data type, λ value, and $\mathcal{B}_{\mathcal{T}}^*$ size. **Right:** Difference between Q-values and mean Q for example states for agents at 500k steps for a single episode rollout, without ACE on the left and with ACE on the right. Shaded regions shows half a standard deviation between seeds, while the dashed lines show the maximum output across the seeds. Value penalization ensures that the maximum stays below 0, verifying that $y(s, s') \leq y(s^*, s^*)$.

VPACE-SQIL can solve all tasks, apart from `relocate-human-v0`, by the final evaluation step. While VPACE-DAC also tends to perform quite well, it is less sample efficient than VPACE-SQIL on average, most likely owing to VPACE-SQIL’s reduced complexity and better discrimination between \mathcal{B} and \mathcal{B}^* . For the Adroit non-DP tasks, VP-SQIL slightly outperforms methods including ACE, while SQIL alone performs comparably to VPACE methods, but we suspect that this is because these tasks have nuances allowing them to be “solved” with very coarse policies that may be undesirable for a real platform (see Appendix D.2 for details). ACE-RCE is consistently outperformed by both VPACE-SQIL and VPACE-DAC, and exhibits higher performance variance. We further examine this result, which conflicts with results presented in [3] showing very poor performance for both SQIL and DAC, in Appendix B. On our real tasks (`RealDrawer` and `RealDoor`), SQIL makes minor progress but is never able to solve either task, while VPACE-SQIL solves both.

Value penalization leads to a dramatic improvement in many of the more complex tasks, but presents comparable results to its exclusion in other tasks. Crucially, there are no tasks where its inclusion *harms* performance. VPACE-SQIL, VPACE-DAC, and ACE-RCE all outperform their single-task counterparts, particularly for the most complex tasks. The improvement for DAC in the simulated Panda environment is particularly stark; reflecting results from [4], DAC learns deceptive rewards for these tasks and, in turn, never learns to complete any of them except for `Reach`.

4.3 Ablations, Data Quantity, and Comparison to Full Trajectories and Sparse Rewards

We completed experiments with many variations from our original implementation of VPACE-SQIL in `Unstack-Stack` (see Fig. 5a). Our main experiments used $\lambda = 10$ for value penalization strength, but we also tested $\lambda = \{1, 100\}$, and found a negligible effect on performance, indicating robustness to λ choice. We tested two different sizes of $\mathcal{B}_{\mathcal{T}}^*$ (for all tasks \mathcal{T} in \mathcal{T}_{all}), $|\mathcal{B}_{\mathcal{T}}^*| = \{10, 100\}$, while the main experiments used $|\mathcal{B}_{\mathcal{T}}^*| = 200$ (following [3]). We found that $|\mathcal{B}_{\mathcal{T}}^*| = 100$ had a negligible effect on performance, but $|\mathcal{B}_{\mathcal{T}}^*| = 10$ slowed learning and impaired final performance. Even with $|\mathcal{B}_{\mathcal{T}}^*| = 10$, VPACE-SQIL outperformed all baselines with $|\mathcal{B}_{\mathcal{T}}^*| = 200$, apart from VPACE-DAC.

A natural question regarding our approach is how its performance compares to more traditional approaches, such as using full expert trajectories and inverse reinforcement learning (IRL), or using RL with true sparse rewards. To test the former, we added full trajectories to each $\mathcal{B}_{\mathcal{T}}^*$ (labelled `+Full Trajectories` in Fig. 5a, `+Full Trajectories & Actions` for learning from actions as well, and `VP-SQIL +Full Trajectories` for single-task only), effectively making our approach similar to [4] but with value-penalization. Intriguingly, peak performance is *reduced* in this setting (especially without ACE), which we hypothesize is because the agent now has to minimize divergence between \mathcal{B} and $\mathcal{B}_{\mathcal{T}}^*$ for many non-successful states, leading to an effect, commonly seen with dense reward functions, known as reward hacking [38]. This result suggests that inverse RL/adversarial IL can be significantly improved by switching to example-based control, but further investigation is required. To test RL with sparse rewards, we removed $\mathcal{B}_{\mathcal{T}}^*$ entirely, and instead use a ground truth $R(s, a)$ from

the environment ($R(s, a)$ already having been used for evaluating success rate), similar to SAC-X [31] with value-penalization. SAC-X (*Sparse Rewards*) does not start accomplishing the main task at all in 500k environment steps, exhibiting substantially poorer performance than VPACE-SQIL and all other baselines (apart from DAC), indicating the high potential utility of immediately and consistently sampling expert success data.

4.4 Value Penalization and Calibration of Q-Values

While our performance results show that value penalization improves performance, they do not explicitly show that $y(s, s') \leq y(s^*, s^*)$ (see Section 3.3). To verify that this goal was met, we took snapshots of each learned agent at 500k steps and ran each policy for a single episode, recording per-timestep Q-values. Instead of showing Q-values directly, we show $Q(s_t, a_t) - \mathbb{E}_{s^* \sim \mathcal{B}^*, a^* \sim \pi(\cdot|s^*)} [Q(s^*, a^*)]$, which should be close to 0 when an episode is completed successfully, and should *never* climb above 0 for $y(s, s') \leq y(s^*, s^*)$ to hold. We show the results of doing so in Unstack-Stack in Fig. 5b (see Appendix E.2 for other tasks).

Both VP-SQIL and VPACE-SQIL clearly do not violate $y(s, s') \leq y(s^*, s^*)$, while both SQIL and ACE-SQIL do. ACE-SQIL, in particular, has *no* values, on average, where $y(s, s') \leq y(s^*, s^*)$, indicating that it has learned poorly calibrated estimates for Q. This is reflected in our main performance results, where, in the most difficult Panda tasks in particular, the improvement from ACE-SQIL to VPACE-SQIL is pronounced. Consequently, scheduled auxiliary control can produce *poorer* policies than its single-task alternative unless it is coupled with value penalization.

5 Limitations

VPACE suffers from several limitations, though many of them are inherited from the use of reinforcement learning and learning from guided play. For an expansion of this section, including these inherited limitations, see Appendix F. In this work, we exclusively learn from numerical state data, rather than raw images, and raw images may be required for tasks involving objects that are not rigid. As well, we claim that example distributions are easier to generate than full expert trajectories, but for certain tasks, generating these example distributions may also be challenging. Finally, tasks we investigate in this work have roughly unimodal example success state distributions, and our method may not gracefully handle multimodality.

6 Conclusion

In this work, we presented VPACE—value-penalized auxiliary control from examples, where we coupled scheduled auxiliary control with value penalization in the example-based setting to significantly improve learning efficiency and stability. Our experiments revealed that scheduled auxiliary control can exacerbate the learning of poorly-calibrated value estimates, which can significantly harm performance, and we alleviated this issue with an approach to value penalization based on the current value estimate of example data. We theoretically showed that our approach to value penalization still affords an optimal policy. We empirically showed that value penalization, together with scheduled auxiliary tasks, greatly improves learning from example states against a set of state-of-the-art baselines, including learning algorithms with other forms of feedback. Opportunities for future work include the further investigation of learned approaches to scheduling, as well as autonomously generating auxiliary task definitions.

Acknowledgments

We gratefully acknowledge the Digital Research Alliance of Canada and NVIDIA Inc., who provided the GPUs used in this work through their Resources for Research Groups Program and their Hardware Grant Program, respectively.

References

- [1] S. Levine, A. Kumar, G. Tucker, and J. Fu. Offline Reinforcement Learning: Tutorial, Review, and Perspectives on Open Problems. *arXiv:2005.01643 [cs, stat]*, May 2020.
- [2] A. Y. Ng and M. I. Jordan. *Shaping and Policy Search in Reinforcement Learning*. PhD thesis, University of California, Berkeley, 2003.
- [3] B. Eysenbach, S. Levine, and R. Salakhutdinov. Replacing Rewards with Examples: Example-Based Policy Search via Recursive Classification, Dec. 2021.
- [4] T. Ablett, B. Chan, and J. Kelly. Learning From Guided Play: Improving Exploration for Adversarial Imitation Learning With Simple Auxiliary Tasks. *IEEE Robotics and Automation Letters*, 8(3):1263–1270, Mar. 2023. ISSN 2377-3766. doi:10.1109/LRA.2023.3236882.
- [5] I. Kostrikov, K. K. Agrawal, D. Dwibedi, S. Levine, and J. Tompson. Discriminator-Actor-Critic: Addressing Sample Inefficiency and Reward Bias in Adversarial Imitation Learning. In *Proceedings of the International Conference on Learning Representations (ICLR’19)*, New Orleans, LA, USA, May 2019.
- [6] S. Reddy, A. D. Dragan, and S. Levine. SQIL: Imitation Learning Via Reinforcement Learning with Sparse Rewards. In *8th International Conference on Learning Representations, ICLR 2020, Addis Ababa, Ethiopia, April 26-30, 2020*. OpenReview.net, 2020.
- [7] A. Gupta, A. Pacchiano, Y. Zhai, S. M. Kakade, and S. Levine. Unpacking Reward Shaping: Understanding the Benefits of Reward Engineering on Sample Complexity. In S. Koyejo, S. Mohamed, A. Agarwal, D. Belgrave, K. Cho, and A. Oh, editors, *Advances in Neural Information Processing Systems 35: Annual Conference on Neural Information Processing Systems 2022, NeurIPS 2022, New Orleans, LA, USA, November 28 - December 9, 2022*, 2022.
- [8] A. Y. Ng, D. Harada, and S. J. Russell. Policy Invariance Under Reward Transformations: Theory and Application to Reward Shaping. In *Proceedings of the Sixteenth International Conference on Machine Learning (ICML’99)*, ICML ’99, pages 278–287, San Francisco, CA, USA, June 1999. Morgan Kaufmann Publishers Inc. ISBN 978-1-55860-612-8.
- [9] I. Popov, N. Heess, T. Lillicrap, R. Hafner, G. Barth-Maron, M. Vecerik, T. Lampe, Y. Tassa, T. Erez, and M. Riedmiller. Data-efficient Deep Reinforcement Learning for Dexterous Manipulation, Apr. 2017.
- [10] C. Berner, G. Brockman, B. Chan, V. Cheung, P. Debiak, C. Dennison, D. Farhi, Q. Fischer, S. Hashme, C. Hesse, R. Józefowicz, S. Gray, C. Olsson, J. Pachocki, M. Petrov, H. P. de Oliveira Pinto, J. Raiman, T. Salimans, J. Schlatter, J. Schneider, S. Sidor, I. Sutskever, J. Tang, F. Wolski, and S. Zhang. Dota 2 with Large Scale Deep Reinforcement Learning. *CoRR*, abs/1912.06680, 2019.
- [11] T. Yu, D. Quillen, Z. He, R. Julian, K. Hausman, C. Finn, and S. Levine. Meta-World: A Benchmark and Evaluation for Multi-Task and Meta Reinforcement Learning. In L. P. Kaelbling, D. Kragic, and K. Sugiura, editors, *3rd Annual Conference on Robot Learning, CoRL 2019, Osaka, Japan, October 30 - November 1, 2019, Proceedings*, volume 100 of *Proceedings of Machine Learning Research*, pages 1094–1100. PMLR, 2019.

- [12] M. Andrychowicz, D. Crow, A. Ray, J. Schneider, R. Fong, P. Welinder, B. McGrew, J. Tobin, P. Abbeel, and W. Zaremba. Hindsight Experience Replay. In I. Guyon, U. von Luxburg, S. Bengio, H. M. Wallach, R. Fergus, S. V. N. Vishwanathan, and R. Garnett, editors, *Advances in Neural Information Processing Systems 30: Annual Conference on Neural Information Processing Systems 2017, December 4-9, 2017, Long Beach, CA, USA*, pages 5048–5058, 2017.
- [13] A. Ng and S. Russell. Algorithms for inverse reinforcement learning. In *International Conference on Machine Learning (ICML'00)*, pages 663–670, July 2000. ISBN 1-55860-707-2. doi:10.2460/ajvr.67.2.323.
- [14] P. Abbeel and A. Y. Ng. Apprenticeship learning via inverse reinforcement learning. In *International Conference on Machine Learning (ICML'04)*, Banff, Alberta, Canada, 2004. ACM Press. doi:10.1145/1015330.1015430.
- [15] B. D. Ziebart, A. L. Maas, J. A. Bagnell, and A. K. Dey. Maximum Entropy Inverse Reinforcement Learning. In D. Fox and C. P. Gomes, editors, *Proceedings of the Twenty-Third AAAI Conference on Artificial Intelligence, AAAI 2008, Chicago, Illinois, USA, July 13-17, 2008*, pages 1433–1438. AAAI Press, 2008. ISBN 9781577353683 (ISBN).
- [16] J. Ho and S. Ermon. Generative Adversarial Imitation Learning. In *Conference on Neural Information Processing Systems*, pages 4565–4573, Barcelona, Spain, Dec. 2016.
- [17] J. Fu, K. Luo, and S. Levine. Learning Robust Rewards with Adversarial Inverse Reinforcement Learning. In *Proceedings of the International Conference on Learning Representations (ICLR'18)*, Vancouver, BC, Canada, Apr. 2018.
- [18] I. Kostrikov, O. Nachum, and J. Tompson. Imitation Learning via Off-Policy Distribution Matching. In *Proceedings of the International Conference on Learning Representations (ICLR'20)*, Virtual, Apr. 2020.
- [19] J. Fu, A. Singh, D. Ghosh, L. Yang, and S. Levine. Variational Inverse Control with Events: A General Framework for Data-Driven Reward Definition. In *Conference on Neural Information Processing Systems*, Montreal, Canada, Dec. 2018.
- [20] T. Haarnoja, A. Zhou, P. Abbeel, and S. Levine. Soft Actor-Critic: Off-Policy Maximum Entropy Deep Reinforcement Learning with a Stochastic Actor. In *Proceedings of the 35th International Conference on Machine Learning (ICML'18)*, pages 1861–1870, Stockholm, Sweden, July 2018.
- [21] A. Singh, L. Yang, K. Hartikainen, C. Finn, and S. Levine. End-to-End Robotic Reinforcement Learning without Reward Engineering. *arXiv:1904.07854 [cs, stat]*, Apr. 2019.
- [22] S. Nasiriany, V. H. Pong, A. Nair, A. Khazatsky, G. Berseth, and S. Levine. DisCo RL: Distribution-Conditioned Reinforcement Learning for General-Purpose Policies, Apr. 2021.
- [23] A. Kumar, A. Zhou, G. Tucker, and S. Levine. Conservative Q-Learning for Offline Reinforcement Learning. In H. Larochelle, M. Ranzato, R. Hadsell, M.-F. Balcan, and H.-T. Lin, editors, *Advances in Neural Information Processing Systems 33: Annual Conference on Neural Information Processing Systems 2020, NeurIPS 2020, December 6-12, 2020, Virtual, 2020*.
- [24] K. B. Hatch, B. Eysenbach, R. Rafailov, T. Yu, R. Salakhutdinov, S. Levine, and C. Finn. Contrastive Example-Based Control. In N. Matni, M. Morari, and G. J. Pappas, editors, *Learning for Dynamics and Control Conference, LADC 2023, 15-16 June 2023, Philadelphia, PA, USA*, volume 211 of *Proceedings of Machine Learning Research*, pages 155–169. PMLR, 2023.
- [25] R. S. Sutton, D. Precup, and S. Singh. Between MDPs and Semi-MDPs: A Framework for Temporal Abstraction in Reinforcement Learning. *Artificial Intelligence*, 112(1-2):181–211, Aug. 1999. ISSN 00043702. doi:10.1016/S0004-3702(99)00052-1.

- [26] R. Fruit, M. Pirootta, A. Lazaric, and E. Brunskill. Regret Minimization in MDPs with Options without Prior Knowledge. In I. Guyon, U. von Luxburg, S. Bengio, H. M. Wallach, R. Fergus, S. V. N. Vishwanathan, and R. Garnett, editors, *Advances in Neural Information Processing Systems 30: Annual Conference on Neural Information Processing Systems 2017, December 4-9, 2017, Long Beach, CA, USA*, pages 3166–3176, 2017.
- [27] Z. Wen, D. Precup, M. Ibrahimi, A. Barreto, B. V. Roy, and S. Singh. On Efficiency in Hierarchical Reinforcement Learning. In H. Larochelle, M. Ranzato, R. Hadsell, M.-F. Balcan, and H.-T. Lin, editors, *Advances in Neural Information Processing Systems 33: Annual Conference on Neural Information Processing Systems 2020, NeurIPS 2020, December 6-12, 2020, Virtual*, 2020.
- [28] A. Robert, C. Pike-Burke, and A. A. Faisal. Sample Complexity of Goal-Conditioned Hierarchical Reinforcement Learning. In A. Oh, T. Naumann, A. Globerson, K. Saenko, M. Hardt, and S. Levine, editors, *Advances in Neural Information Processing Systems 36: Annual Conference on Neural Information Processing Systems 2023, NeurIPS 2023, New Orleans, LA, USA, December 10 - 16, 2023*, 2023.
- [29] A. Nair, B. McGrew, M. Andrychowicz, W. Zaremba, and P. Abbeel. Overcoming Exploration in Reinforcement Learning with Demonstrations. In *Proceedings of the 2018 IEEE International Conference on Robotics and Automation (ICRA'18)*, pages 6292–6299, Brisbane, Australia, May 2018. doi:10.1109/ICRA.2018.8463162.
- [30] O. Nachum, H. Tang, X. Lu, S. Gu, H. Lee, and S. Levine. Why Does Hierarchy (Sometimes) Work So Well in Reinforcement Learning? In *Proceedings of the Neural Information Processing Systems (NeurIPS'19) Deep Reinforcement Learning Workshop*, Sept. 2019.
- [31] M. Riedmiller, R. Hafner, T. Lampe, M. Neunert, J. Degraeve, T. Wiele, V. Mnih, N. Heess, and J. T. Springenberg. Learning by Playing Solving Sparse Reward Tasks from Scratch. In *Proceedings of the 35th International Conference on Machine Learning (ICML'18)*, pages 4344–4353, Stockholm, Sweden, July 2018.
- [32] T. Ablett, B. Chan, and J. Kelly. Learning from Guided Play: A Scheduled Hierarchical Approach for Improving Exploration in Adversarial Imitation Learning. In *Proceedings of the Neural Information Processing Systems (NeurIPS'21) Deep Reinforcement Learning Workshop*, Dec. 2021.
- [33] G. Xiang, S. Li, F. Shuang, F. Gao, and X. Yuan. SC-AIRL: Share-Critic in Adversarial Inverse Reinforcement Learning for Long-Horizon Task. *IEEE Robotics and Automation Letters*, 9(4): 3179–3186, Apr. 2024. ISSN 2377-3766. doi:10.1109/LRA.2024.3366023.
- [34] W.-D. Chang, S. Fujimoto, D. Meger, and G. Dudek. Imitation Learning from Observation through Optimal Transport, Oct. 2023.
- [35] F. Torabi. Imitation Learning from Observation. In *Proceedings of the AAAI Conference on Artificial Intelligence*, volume 33, pages 9900–9901, July 2019. doi:10.1609/aaai.v33i01.33019900.
- [36] F. Pardo, A. Tavakoli, V. Levdiuk, and P. Kormushev. Time Limits in Reinforcement Learning. In J. G. Dy and A. Krause, editors, *Proceedings of the 35th International Conference on Machine Learning, ICML 2018, Stockholm, Sweden, July 10-15, 2018*, volume 80 of *Proceedings of Machine Learning Research*, pages 4042–4051. PMLR, 2018.
- [37] A. Rajeswaran*, V. Kumar*, A. Gupta, G. Vezzani, J. Schulman, E. Todorov, and S. Levine. Learning Complex Dexterous Manipulation with Deep Reinforcement Learning and Demonstrations. In *Proceedings of Robotics: Science and Systems (RSS'18)*, Pittsburgh, PA, USA, June 2018.

- [38] J. Skalse, N. Howe, D. Krasheninnikov, and D. Krueger. Defining and characterizing reward gaming. In S. Koyejo, S. Mohamed, A. Agarwal, D. Belgrave, K. Cho, and A. Oh, editors, *Advances in Neural Information Processing Systems*, volume 35, pages 9460–9471. Curran Associates, Inc., 2022.
- [39] M. Vecerik, T. Hester, J. Scholz, F. Wang, O. Pietquin, B. Piot, N. Heess, T. Rothörl, T. Lampe, and M. Riedmiller. Leveraging Demonstrations for Deep Reinforcement Learning on Robotics Problems with Sparse Rewards, Oct. 2018.
- [40] B. Scherrer. Improved and Generalized Upper Bounds on the Complexity of Policy Iteration. In C. J. C. Burges, L. Bottou, Z. Ghahramani, and K. Q. Weinberger, editors, *Advances in Neural Information Processing Systems 26: 27th Annual Conference on Neural Information Processing Systems 2013. Proceedings of a Meeting Held December 5-8, 2013, Lake Tahoe, Nevada, United States*, pages 386–394, 2013.
- [41] T. Zhang. *Mathematical Analysis of Machine Learning Algorithms*. Cambridge University Press, Cambridge, 2023. doi:10.1017/9781009093057.
- [42] B. Scherrer, M. Ghavamzadeh, V. Gabillon, B. Lesner, and M. Geist. Approximate modified policy iteration and its application to the game of Tetris. *Journal of Machine Learning Research*, 16:1629–1676, 2015. doi:10.5555/2789272.2886802.
- [43] S. Garrido-Jurado, R. Muñoz-Salinas, F. Madrid-Cuevas, and M. Marín-Jiménez. Automatic generation and detection of highly reliable fiducial markers under occlusion. *Pattern Recognition*, 47(6):2280–2292, June 2014. ISSN 00313203. doi:10.1016/j.patcog.2014.01.005.
- [44] Y. Lin, A. S. Wang, G. Sutanto, A. Rai, and F. Meier. Polymetis. <https://facebookresearch.github.io/fairo/polymetis/>, 2021.
- [45] S. K. S. Ghasemipour, R. S. Zemel, and S. S. Gu. A Divergence Minimization Perspective on Imitation Learning Methods. In *Conference on Robot Learning (CoRL'19)*, 2019.
- [46] B. Chan. RL sandbox. https://github.com/chanb/rl_sandbox_public, 2020.
- [47] D. Yarats, R. Fergus, A. Lazaric, and L. Pinto. Mastering Visual Continuous Control: Improved Data-Augmented Reinforcement Learning. In *The Tenth International Conference on Learning Representations, ICLR 2022, Virtual Event, April 25-29, 2022*. OpenReview.net, 2022.
- [48] S. Sinha, A. Mandlekar, and A. Garg. S4RL: Surprisingly Simple Self-Supervision for Offline Reinforcement Learning. In *Conference on Robot Learning (CoRL'21)*, London, UK, Nov. 2021.
- [49] X. Chen, C. Wang, Z. Zhou, and K. Ross. Randomized Ensembled Double Q-Learning: Learning Fast Without a Model. *arXiv:2101.05982 [cs]*, Mar. 2021.

A Reward Model Formulations

In this section, we investigate approaches to off-policy reinforcement learning (RL) studied in this work, modified to accommodate an unknown R and the existence of an example state buffer \mathcal{B}^* .

A.1 Learning a Reward Function

The most popular approach to reward modelling, known as inverse RL, tackles an unknown R by explicitly learning a reward model. Modern approaches under the class of adversarial imitation learning (AIL) algorithm aim to learn both the reward function and the policy simultaneously. In AIL, the learned reward function, also known as the discriminator, aims to differentiate the occupancy measure between the state-action distributions induced by expert and the learner. In example-based control, the state-conditional discriminator loss is Eq. (3), where D attempts to differentiate the occupancy measure between the state distributions induced by \mathcal{B}^* and \mathcal{B} . The output of $D(s)$ is used to define $\hat{R}(s)$, which is then used for updating the Q-function using Eq. (6).

In example-based control, the discriminator D provides a smoothed label of success for states, thus its corresponding reward function can provide more density than a typical sparse reward function, making this approach an appealing choice. Unfortunately, a learned discriminator can suffer from the deceptive reward problem, as previously identified in [4], and this problem is exacerbated in the example-based setting. In the following sections, we describe options to remove the reliance on separately learned discriminators.

A.2 Discriminator-Free Reward Labels with Mean Squared Error TD Updates

A simple alternative to using a discriminator as a reward model was initially introduced as soft-Q imitation learning (SQIL) in [6]. In standard AIL algorithms, D is trained separately from π and Q^π , where D is trained using data from both \mathcal{B} and \mathcal{B}^* , whereas π and Q^π are trained using data exclusively from \mathcal{B} . However, most off-policy algorithms do not *require* this choice, and approaches such as [4, 39] train Q , and possibly π , using data from both \mathcal{B} and \mathcal{B}^* . It is unclear why this choice is often avoided in AIL, but it might be because it can introduce instability due to large discrepancy in magnitudes for Q targets given data from \mathcal{B} and \mathcal{B}^* . Sampling from both buffers, we can define $\hat{R}(s_t, a_t)$ in Eq. (2) to be labels corresponding to whether the data is sampled from \mathcal{B} or \mathcal{B}^* —in SQIL, the labels are respectively 0 and 1. The full training objective resembles the minimax objective in Eq. (3) where we set $D(s^*) = 1$ and $D(s) = 0$.

The resulting reward function is the expected label $\hat{R}(s, a) = \mathbb{E}_{\hat{\mathcal{B}} \sim \text{Categorical}_s(\{\mathcal{B}, \mathcal{B}^*\})} [\mathbf{1}(\hat{\mathcal{B}} = \mathcal{B}^*)]$, where Categorical_s is a categorical distribution corresponding to the probability that s belongs to buffers $\mathcal{B}, \mathcal{B}^*$. Consequently, only successful states s^* yields positive reward and the corresponding optimal policy will aim to reach a successful state as soon as possible. If we further assume that s^* transitions to itself, then for policy evaluation with mean-squared error (MSE), we can write the temporal difference (TD) target, y , of Q-updates with:

$$y(s, s') = \gamma \mathbb{E}_{a'} [Q(s', a')], \quad (11) \quad y(s^*, s^*) = 1 + \gamma \mathbb{E}_{a'} [Q(s^*, a')], \quad (12)$$

where $(s, \cdot, s') \sim \mathcal{B}$, $a' \sim \pi(a'|s')$, and $s^* \sim \mathcal{B}^*$.

This approach reduces complexity as we no longer explicitly train a reward model, and also guarantees discrimination between data from \mathcal{B} and \mathcal{B}^* .

A.3 Discriminator-Free Reward Labels with Binary Cross Entropy TD Updates

Eysenbach et al. [3] introduced recursive classification of examples (RCE), a method for learning from examples of success. RCE mostly follows the approach outlined above in Appendix A.2 but

uses a weighted binary cross-entropy (BCE) loss with weights $1 + \gamma w$ for data from \mathcal{B} and $1 - \gamma$ for data from \mathcal{B}^* . The TD targets are also changed from Eq. (11) and Eq. (12) to

$$y(s, s') = \gamma w(s') / (1 + \gamma w(s')), \quad (13) \qquad y(s^*, s^*) = 1, \quad (14)$$

where $w(s') = V^\pi(s') / (1 - V^\pi(s'))$.

This approach can also be made closer to SQIL by removing the change in weights and by leaving Eq. (13) as Eq. (11). This makes it equivalent to SQIL, apart from removing bootstrapping from Eq. (12), and using a BCE instead of MSE for TD updates.

A major benefit of this approach, compared with the MSE TD updates in Appendix A.2, is that $y(s, s') \leq y(s^*, s^*)$ is always enforced at every update, meaning that our approach to value penalization would provide no extra benefit. Nonetheless, our results from Appendix B show that SQIL, even *without* value-penalization, almost always outperforms both RCE and SQIL with BCE loss (referred to SQIL-BCE here).

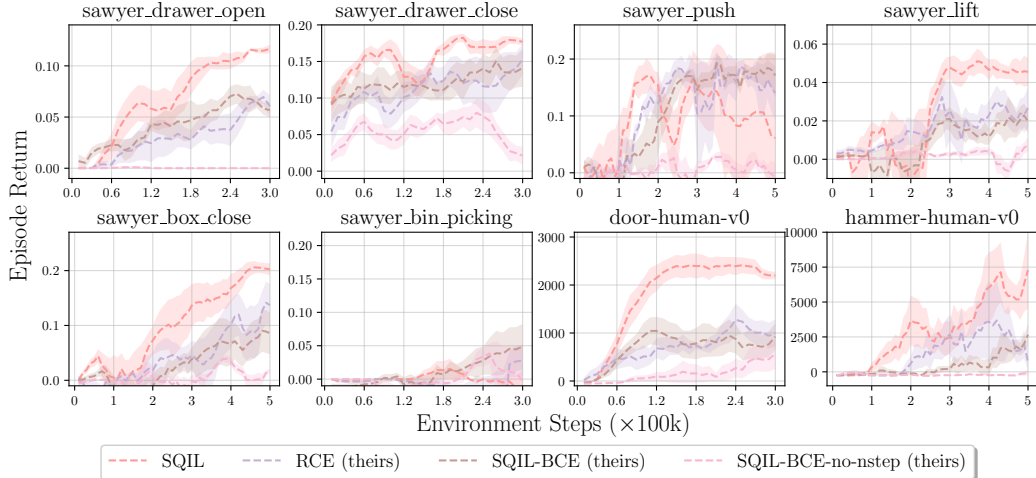


Figure 6: Performance results on the Sawyer and Adroit tasks considered in [3], using their own implementations based on binary cross entropy (BCE) loss, but with an additional SQIL-BCE (including n -step) baseline. We also show our implementation of SQIL (without value penalization or auxiliary tasks), with Mean Squared Error TD updates, which outperforms all of the BCE-based methods on average.

B Why Does SQIL Outperform RCE?

Our results show that VPACE-SQIL outperforms ACE-RCE, and that VP-SQIL and SQIL outperform RCE in almost all cases. This result is in conflict with results from [3], which showed SQIL strongly outperformed by RCE. In this section, we show results that help explain our findings.

Eysenbach et al. [3] claimed that the highest performing baseline against RCE was SQIL, but it is worth noting that their implementation¹ is a departure from the original SQIL implementation, which uses MSE for TD updates, described in Appendix A.2. Furthermore, Eysenbach et al. [3] also noted that it was necessary to add n -step returns to off-policy learning to get reasonable performance. In their experiments, however, this adjustment was not included for their version of SQIL with BCE loss. We complete the experiments using their implementation and show the average results across all RCE environments in Fig. 6, and also compare to using SQIL with MSE (without value penalization or auxiliary tasks) for TD updates.

These results empirically show that RCE and SQIL with BCE loss perform nearly identically, indicating that benefits of the changed TD targets and weights described in Appendix A.3 may not be as clear as previously described. Furthermore, SQIL with MSE clearly performs better on average, although it still performs worse than VPACE (see Appendix E). While these empirical results demonstrate that example-based control with BCE loss for TD updates is outperformed by SQIL with MSE, Eysenbach et al. [3] had theoretical results indicating that RCE should still learn an optimal policy. In the following section, we describe a flaw found in one of their proofs that may help to further understand why RCE is outperformed by SQIL with MSE.

B.1 Re-Examination of the Proofs from Section 4 of RCE [3]

In this section, we outline potential flaws in the proofs of Lemma 4.2 and Corollary 4.2.1 in RCE [3]. We then provide a lemma that shows RCE can be considered as recovering a specific reward function, thereby unifying RCE with other IRL algorithms.

To begin, recall that the RCE objective (i.e. Eq. (7) of Eysenbach et al. [3]) is defined as follows:

$$\mathcal{L}^\pi(\theta) := p(e_{t+} = 1) \mathbb{E}_{p(s_t, a_t | e_{t+} = 1)} [\log C_\theta^\pi(s_t, a_t)] + \mathbb{E}_{p(s_t, a_t)} [\log(1 - C_\theta^\pi(s_t, a_t))]. \quad (15)$$

¹Available at <https://github.com/google-research/google-research/tree/master/rce> at time of writing.

Eysenbach et al. [3] stated the following Lemma and Corollary to demonstrate that optimizing Eq. (15) is equivalent to value iteration under the tabular setting:

Lemma 1. (Lemma 4.2 of RCE) *In the tabular setting, the expected updates for Eq. (15) are equivalent to performing value iteration with reward function $r(s_t, a_t) = (1 - \gamma)p(e_t = 1|s_t)$ and a Q -function parameterized as $Q_\theta^\pi(s_t, a_t) = \frac{C_\theta^\pi(s_t, a_t)}{1 - C_\theta^\pi(s_t, a_t)}$.*

Corollary 1. (Corollary 4.2.1 of RCE) *RCE converges in the tabular setting.*

In Lemma 1, we find that the proof intends to demonstrate equivalence with policy evaluation. In particular, the temporal difference (TD) target is defined to be $y = r(s, a) + \gamma\mathbb{E}_{s', a'} [Q(s', a')]$, which is optimizing the Bellman **expected** equation rather than Bellman **optimal** equation. Furthermore, the assignment equation for the ratio should in fact be an expectation over both the next state-and-action pairs (i.e. $s_{t+1} \sim p(\cdot|s_t, a_t)$ and $a_{t+1} \sim \pi(\cdot|s_{t+1})$) instead of only the next state, even if we aim to perform policy evaluation. As a result, Corollary 1 also fails to hold if we simply use the convergence proof of value iteration.

We now provide a lemma indicating that the optimal solution of Eq. (15) is equivalent to finding Q^π with reward $r(s, a) = (1 - \gamma)p^\pi(e = 1|s)$:

Lemma 2. *Fix any policy $\pi : \mathcal{S} \rightarrow \Delta(\mathcal{A})$. Let $\theta^* = \arg \min_\theta \mathcal{L}^\pi(\theta)$ be the optimal solution of Eq. (15). Consider an MDP with reward function $r(s_t, a_t) = (1 - \gamma)p(e_t = 1|s_t, a_t)$. Then, in the tabular setting, $Q^\pi = \frac{C^\pi}{1 - C^\pi}$ satisfies the Bellman expected equation. Furthermore, we have that $Q^\pi(s_t, a_t) = p^\pi(e_{t+} = 1|s_t, a_t)$. That is, the solution of Eq. (15) is equivalent to finding Q^π .*

Proof. Fix any policy π . Consider an MDP with reward function $r(s, a) = (1 - \gamma)p(e = 1|s)$ and transition function $p(s'|s, a)$. We define the Bellman expected operator $\mathcal{T}^\pi : \mathbb{R}^{\mathcal{S} \times \mathcal{A}} \rightarrow \mathbb{R}^{\mathcal{S} \times \mathcal{A}}$ to be

$$\mathcal{T}^\pi q(s, a) := r(s, a) + \gamma\mathbb{E}_{s' \sim p(\cdot|s, a), a' \sim \pi(\cdot|s)} [q(s', a')].$$

Note that under the tabular setting, \mathcal{T}^π is a γ -contraction mapping under max-norm [40]. Thus, by Banach fixed-point theorem, we have that for any $q \in \mathbb{R}^{\mathcal{S} \times \mathcal{A}}$,

$$Q^\pi = (\mathcal{T}^\pi)^\infty q.$$

In other words, performing policy evaluation on π with reward $r(s, a) = (1 - \gamma)p(e = 1|s)$ yields Q^π . Now, by Lemma 4.1 of Eysenbach et al. [3], we have that

$$\frac{C^\pi(s_t, a_t)}{1 - C^\pi(s_t, a_t)} = (1 - \gamma)p(e_t = 1|s_t) + \gamma\mathbb{E}_{s_{t+1} \sim p(\cdot|s_t, a_t), a_{t+1} \sim \pi(\cdot|s_t)} \left[\frac{C^\pi(s_{t+1}, a_{t+1})}{1 - C^\pi(s_{t+1}, a_{t+1})} \right]. \quad (16)$$

Eq. (16) satisfies the Bellman expected equation, thus by uniqueness of the fixed-point theorem, we have that

$$Q^\pi(s_t, a_t) = \frac{C^\pi(s_t, a_t)}{1 - C^\pi(s_t, a_t)}.$$

Recall that $\frac{C^\pi(s_t, a_t)}{1 - C^\pi(s_t, a_t)}$ is the Bayes' optimal classifier for Eq. (15). Therefore, suppose we obtain the minimum of Eq. (15), that is, $\theta^* = \arg \min_\theta \mathcal{L}^\pi(\theta)$, then we have that

$$p(e_{t+} = 1|s_t, a_t) = \frac{C_{\theta^*}^\pi(s_t, a_t)}{1 - C_{\theta^*}^\pi(s_t, a_t)} = \frac{C^\pi(s_t, a_t)}{1 - C^\pi(s_t, a_t)} = Q^\pi(s_t, a_t),$$

meaning that finding the minimum of $\mathcal{L}^\pi(\theta)$ is equivalent to performing policy evaluation on π . \square

With Lemma 2 and Lemma 4.3 of [3], we can view Algorithm 1 of Eysenbach et al. [3] as a form of policy iteration under the reward function $r(s, a) = (1 - \gamma)p(e = 1|s)$, where (i) updating the classifier θ corresponds to performing a policy evaluation step on π , and (ii) updating the policy π corresponds to performing a policy improvement step. We note that, however, the RCE objective is not necessarily equivalent to policy evaluation when the true minimum of RCE, θ^* , is not obtained.

C Finite-Sample Analysis of Value-Penalty Regularization

In this section, we show a finite-sample complexity bound of learning the Q-function via mean-squared error (MSE) with value-penalty regularization and demonstrate that we can use its solution for approximate policy iteration (API). Intuitively, given a fixed set of samples, a near-optimal solution obtained using the regularized loss is closed to the true optimal solution of the unregularized loss with high probability. Then, if we can control the error of the solution from the regularized loss, we can further bound the value error between the Q-function output by API and the optimal Q-function.

More formally, consider a parameterized function class $\mathcal{Q} = \{Q_\theta : \mathbb{R}^{\mathcal{S} \times \mathcal{A}} \rightarrow \mathbb{R} \mid \theta \in \Theta\}$. We define the MSE as

$$\ell(\theta, Z_N) = \frac{1}{N} \sum_{n=1}^N (Q_\theta(S_n, A_n) - G_n)^2, \quad (17)$$

where $Z_N = \{(S_n, A_n, G_n)\}_{n=1}^N$ is N samples of the state-action pairs and the corresponding expected return. The value-penalty regularizer is defined as

$$h(\theta, Z_n) = \lambda \frac{1}{N} \sum_{n=1}^N (\max(Q_\theta(S_n, A_n) - Q_U, 0))^2 + (\max(Q_L - Q_\theta(S_n, A_n), 0))^2, \quad (18)$$

for some constants $Q_L < Q_U$, corresponding to the lowest and highest possible Q-values respectively, and positive constant λ . Then, the MSE with value-penalty regularization is defined as

$$\ell_{reg}(\theta, Z_N) = \ell(\theta, Z_N) + h(\theta, Z_N). \quad (19)$$

During training, suppose we are given N i.i.d. samples Z_N from \mathcal{D} . We aim to approximate the regularized empirical risk minimizer (ERM) to obtain $\hat{\theta}$:

$$\ell(\hat{\theta}, Z_n) + h(\hat{\theta}, Z_n) \leq \min_{\theta \in \Theta} [\ell(\theta, Z_n) + h(\theta, Z_n)] + \varepsilon'. \quad (20)$$

Our goal is to find the approximate regularized ERM $\hat{\theta}$ that achieves a low test loss, defined by

$$\mathcal{L}(\theta, \mathcal{D}) = \mathbb{E}_{Z \sim \mathcal{D}} [\ell(\theta, Z)]. \quad (21)$$

To begin, we assume that the function class has bounded outputs (or bounded parameters) which is a standard requirement for characterizing generalization errors:

Assumption 1. (*Bounded function output and realizability.*) Let $C_{\mathcal{Q}} \geq \max(|Q_L|, |Q_U|)$. The parameterized function class \mathcal{F} is bounded: $\mathcal{Q} = \{Q_\theta : \mathbb{R}^{\mathcal{S} \times \mathcal{A}} \rightarrow [-C_{\mathcal{Q}}, C_{\mathcal{Q}}] \mid \theta \in \Theta\}$. Moreover, the optimal parameter of the test loss belongs to the function class: $\theta^* = \arg \min_{\theta} \mathcal{L}(\theta, \mathcal{D}) \in \Theta$.

Note that the regularizer term Eq. (18) only has an effect when the function Q_θ predicts values that are out-of-range, therefore we set $C_{\mathcal{Q}}$ to be larger than the maximum possible returns for a more meaningful analysis, otherwise we recover the unregularized loss Eq. (17). Furthermore, we characterize the complexity of the function class \mathcal{Q} using the expected Rademacher complexity with offset.

Definition 1. The expected Rademacher complexity is defined to be

$$\mathfrak{R}_N^h(\mathcal{Q}, \mathcal{D}) = \mathbb{E}_{Z_N \sim \mathcal{D}} \left[\mathbb{E}_\sigma \left[\sup_{\theta \in \Theta} \frac{1}{N} \sum_{n=1}^N \sigma_n (\ell(\theta, Z_n) + 0.5h(\theta, Z_n)) - 0.5h(\theta, Z_n) \right] \right],$$

where $\sigma_1, \dots, \sigma_N$ are independent Rademacher random variables.

Then, by Corollary 6.21 of [41], we can show that the approximate ERM satisfies the oracle inequality with high probability, which we state here:

Lemma 3. (Corollary 6.21 of [41].) Let $\Delta_N h(\theta) \leq \sup_{z, z'} [h(\theta, z) - h(\theta, z')]$. Assume that for some $C \geq 0$:

$$\sup_{\theta \in \Theta} \left[\sup_{z, z'} [\ell(\theta, z) - \ell(\theta, z') + \Delta_N h(\theta)] \right] \leq C.$$

Then the approximate ERM specified by Eq. (20), $\hat{\theta}$, satisfies the following oracle inequality. For any $\delta, \delta' > 0$, with probability $1 - \delta - \delta'$, we have that

$$\begin{aligned} \mathcal{L}(\hat{\theta}, \mathcal{D}) &\leq \inf_{\theta \in \Theta} \left[\mathcal{L}(\theta, \mathcal{D}) + \mathbb{E}_{Z_n} [h(\theta, Z_N)] + \Delta_N h(\theta) \sqrt{\frac{\log(1/\delta')}{2N}} \right] \\ &\quad + \varepsilon' + 2\mathfrak{R}_N^h(\mathcal{Q}, \mathcal{D}) + 2C \sqrt{\frac{\log(1/\delta)}{2N}}. \end{aligned}$$

We note that the first term of RHS in Lemma 3 is zero due to Assumption 1. In particular, by Assumption 1 and uniqueness of Bellman expected operator, we have that $\mathcal{L}(\theta^*, \mathcal{D}) = 0$. The second term $\mathbb{E}_{Z_n} [h(\theta, Z_N)] = 0$ and the first factor in the third term $\Delta_N h(\theta) = 0$ since Q_{θ^*} is a valid Q-function, thus no clipping is applied. Without loss of generality, suppose that $\varepsilon' = 0$, then by Lemma 3 we have that with probability $1 - \delta - \delta'$,

$$\mathcal{L}(\hat{\theta}, \mathcal{D}) \leq 2\mathfrak{R}_N^h(\mathcal{Q}, \mathcal{D}) + 2C \sqrt{\frac{\log(1/\delta)}{2N}} = \|\varepsilon_{\text{approx}}\|_{2, \mathcal{D}}.$$

In other words, as we increase the number of samples N , the approximation error of $\hat{\theta}$, $\|\varepsilon_{\text{approx}}\|_{2, \mathcal{D}}$, approaches zero with high probability. The boundedness in Assumption 1 further ensures that the Rademacher complexity is well-behaved and shrinks to zero as N increases under the test loss [41].

Now, consider the approximate policy iteration algorithm for Q-function called AMPI-Q [42]. Instead of approximating the Q-function using the standard squared-loss Eq. (17), we instead use the regularized loss Eq. (19). From Lemma 3 we know that $\mathcal{L}(\hat{\theta}, \mathcal{D}) \leq \|\varepsilon_{\text{approx}}\|_{2, \mathcal{D}}$ with high probability. Consequently, at each iteration k of AMPI-Q, we can replace the policy evaluation error $\|\varepsilon_k\|_{2, \mu}$ with $\|\varepsilon_{\text{approx}}\|_{2, \mathcal{D}}$ and immediately obtain a finite-sample analysis of AMPI-Q through Theorem 8 of [42].

Theorem 1. With Assumption 1 and the assumptions from [42], after k iterations, AMPI-Q with regularized loss Eq. (19) for policy evaluation satisfies the following with probability $1 - \delta - \delta'$:

$$\|Q^* - Q^{\pi_k}\|_{2, \rho_0} \leq \frac{2(\gamma - \gamma^k)(\mathcal{C}_\infty^{1, k, 0})^{\frac{1}{2}}}{(1 - \gamma)^2} \left(2\mathfrak{R}_N^h(\mathcal{Q}, \mathcal{D}) + 2C \sqrt{\frac{\log(k/\delta)}{2N}} \right) + g(k),$$

where $\mathcal{C}_\infty^{1, k, 0}$ and $g(k)$ are the concentrability-coefficients related terms defined in [42].

Proof. We can directly apply Theorem 8 of [42] (setting $p = 2, q' = 1, q = \infty$) and take the union bound over the bad events, that is, with probability at most $(\delta + \delta')/k$, $\mathcal{L}(\hat{\theta}, \mathcal{D}) > \|\varepsilon_{\text{approx}}\|_{2, \mathcal{D}}$ for each of k iterations. \square

Theorem 1 indicates that when we run AMPI-Q for sufficiently large number of iterations, the learned policy reaches optimal policy performance, even when using our proposed value-penalty regularization Eq. (18) on the standard squared loss for policy evaluation.

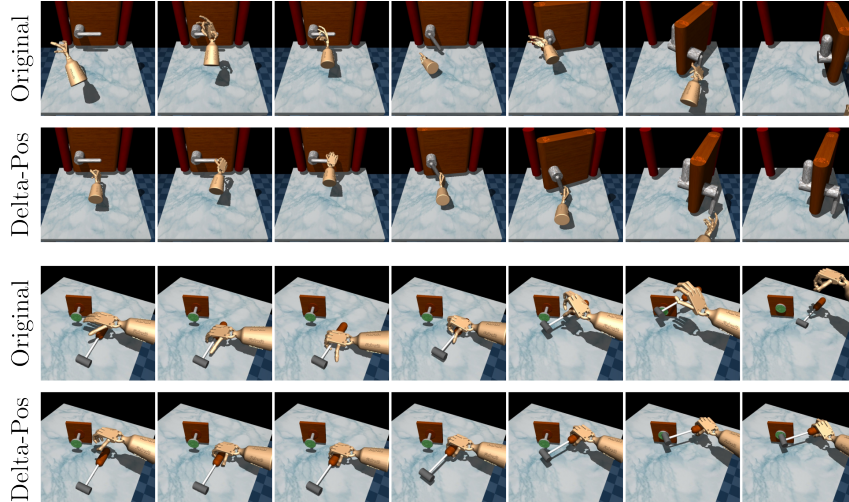


Figure 7: Learned VPACE-SQL policies at the final training step for, from top to bottom, `door-human-v0`, `door-human-v0-dp`, `hammer-human-v0`, and `hammer-human-v0-dp`. Although the original versions of the environments are solved, the absolute position action space allows policies to execute very coarse actions that exploit the simulator (above, hitting the handle without grasping it and throwing the hammer, respectively), and would almost certainly cause damage to a real environment.

D Additional Environment, Algorithm, and Implementation Details

The following sections contain further details of the environments, tasks, auxiliary tasks, algorithms, and implementations used in our experiments.

D.1 Additional Environment Details

Compared with the original Panda tasks from LfGP [4], we switch from 20Hz to 5Hz control (finding major improvements in performance for doing so), improve handling of rotation symmetries in the observations, and remove the force-torque sensor since it turned out to have errors at low magnitudes. Crucially, these modifications did not require training new expert policies, since the same final observation states from the full trajectory expert data from [4] remained valid. Compared with the original LfGP tasks, we also remove `Move-block` as an auxiliary task from `Stack`, `Unstack-Stack`, `Bring` and `Insert`, since we found a slight performance improvement for doing so, and add `Reach`, `Lift`, and `Move-block` as main tasks. The environment was otherwise identical to how it was implemented in LfGP, including allowing randomization of the block and end-effector positions anywhere above the tray, using delta-position actions, and using end-effector pose, end-effector velocity, object pose, object velocity, and relative positions in the observations. For even further details of the original environment, see [4].

Since the Sawyer tasks from [3, 11] only contain end-effector position and object position by default, they do not follow the Markov property. To mitigate this, we train all algorithms in the Sawyer tasks with frame-stacking of 3 and add in gripper position to the observations, since we found that this, at best, improved performance for all algorithms, and at worst, kept performance the same. We validate that this is true by also performing experiments using the original code and environments from [3], unmodified, where the results of RCE without these modifications are presented in Fig. 6, with results comparable to or poorer than our own RCE results.

D.2 Delta-Position Adroit Hand Environments

The Adroit hand tasks from [37] use absolute positions for actions. This choice allows even very coarse policies, with actions that would be unlikely to be successful in the real world, to learn to complete `door-human-v0` and `hammer-human-v0`, and also makes the intricate exploration re-

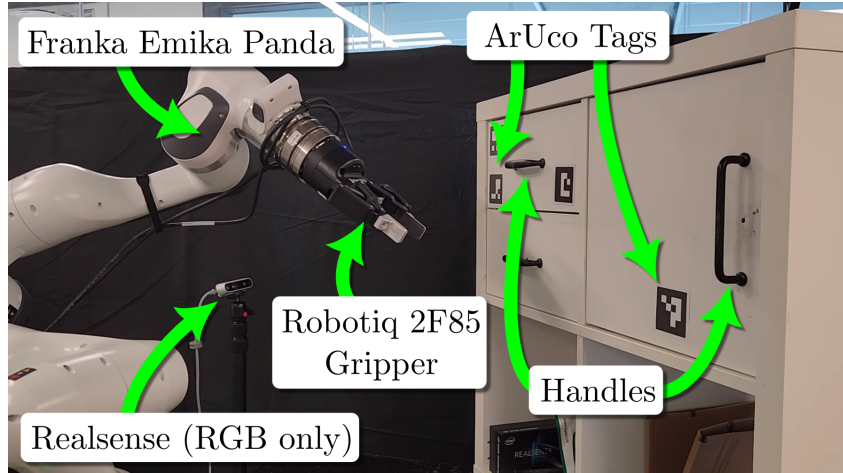


Figure 8: Experimental setup for our real environment and our RealDrawer and RealDoor tasks. The robot has a force-torque sensor attached, but it is not used for our experiments.

quired to solve `relocate-human-v0` very difficult. Specifically, VPACE-SQIL and several other baselines achieve high return in `door-human-v0` and `hammer-human-v0`, but the learned policies use unrealistic actions that exploit simulator bugs. As well, no methods are able to achieve any return in `relocate-human-v0` in 1.5M environment steps.

In the interest of solving `relocate-human-v0` and learning more skillful policies, we generated modified versions of these environments with delta-position action spaces. Furthermore, in `relocate-human-v0-najp-dp`, the action space rotation frame was changed to be in the palm, rather than at the elbow, and, since relative positions between the palm, ball, and relocate goal are included as part of the state, we removed the joint positions from the state. In our experiments, these modified environments were called `door-human-v0-dp`, `hammer-human-v0-dp`, and `relocate-human-v0-najp-dp`. See Fig. 7 for a comparison of learned policies in each version of these environments.

D.3 Real World Environment Details

Fig. 8 shows our experimental platform and setup for our two real world tasks. In both RealDrawer and RealDoor, the observation space contains the end-effector position, an ArUco tag [43] to provide drawer or door position (in the frame of the RGB camera; we do not perform extrinsic calibration between the robot and the camera), and the gripper finger position. The action space in both contains delta-positions and a binary gripper command for opening and closing. The action space for RealDrawer is one-dimensional (allowing motion in a line), while the action space for RealDoor is two-dimensional (allowing motion in a plane). The initial state distribution for RealDrawer allows for initializing the end-effector anywhere within a 10 cm line approximately 25 cm away from the drawer handle when closed. For RealDoor, the initial state distribution is a 20 cm \times 20 cm square, approximately 20cm away from the door handle when closed. Actions are supplied at 5 Hz.

For both environments, for evaluation only, success is determined by whether the drawer or door is fully opened, as detected by the absolute position of the ArUco tag in the frame of the RGB camera. Our robot environment code is built on Polymetis [44], and uses the default hybrid impedance controller that comes with the library. To reduce environmental damage from excessive forces and torques, we reduced Cartesian translational stiffness in all dimensions from 750 N/m to 250 N/m, and the force and torque limits in all dimensions from 40 N and 40 Nm to 20 N and 20 Nm.

Algorithm	Value Penalization	Sched. Aux. Tasks	Reward Model	TD Error Loss	Source
VPACE-SQIL	✓	✓	SQIL	MSE	Ours
ACE-SQIL	✗	✓	SQIL	MSE	Ours
VPACE-DAC	✓	✓	DAC	MSE	Ours
ACE-RCE	✗	✓	RCE	BCE	Ours
VP-SQIL	✓	✗	SQIL	MSE	Ours
VP-DAC	✓	✗	DAC	MSE	Ours
SQIL	✗	✗	SQIL	MSE	Ours
RCE	✗	✗	RCE	BCE	Ours
RCE (theirs)	✗	✗	RCE	BCE	[3]
SQIL-BCE	✗	✗	SQIL	BCE	[3]

Table 1: Major differences between algorithms studied in this work. MSE refers to mean squared error, while BCE refers to binary cross entropy.

D.4 Additional Task Details

Fig. 9 shows representative images for all environments and tasks used in this work. Success examples for the Panda environments were gathered by taking s_T from the existing datasets provided by [4]. Success examples for main tasks from the Sawyer environments were generated using the same code from [3], in which the success examples were generated manually given knowledge of the task. Auxiliary task data was generated with a similar approach. Success examples for the Adroit hand environments were generated from the original human datasets provided by [37]. Success examples for our real world tasks were generated by manually moving the robot to a small set of successful positions for each auxiliary task and main task.

As stated in Section 4.1, all Panda main tasks use the the auxiliary tasks *release*, *reach*, *grasp*, and *lift*.

There are two specific nuances that were left out of the main text for clarity and brevity: (i) the *Reach* main task only uses *release* as an auxiliary task (since it also acts as a “coarse” reach), and (ii) half of the *release* dataset for each task is specific to that task (e.g., containing insert or stack data), as was the case in the original datasets from [4]. For the Sawyer, Hand, and real Panda environments, because the observation spaces are not shared, each task has its own separate *reach* and *grasp* data.

D.5 Additional Algorithm Details

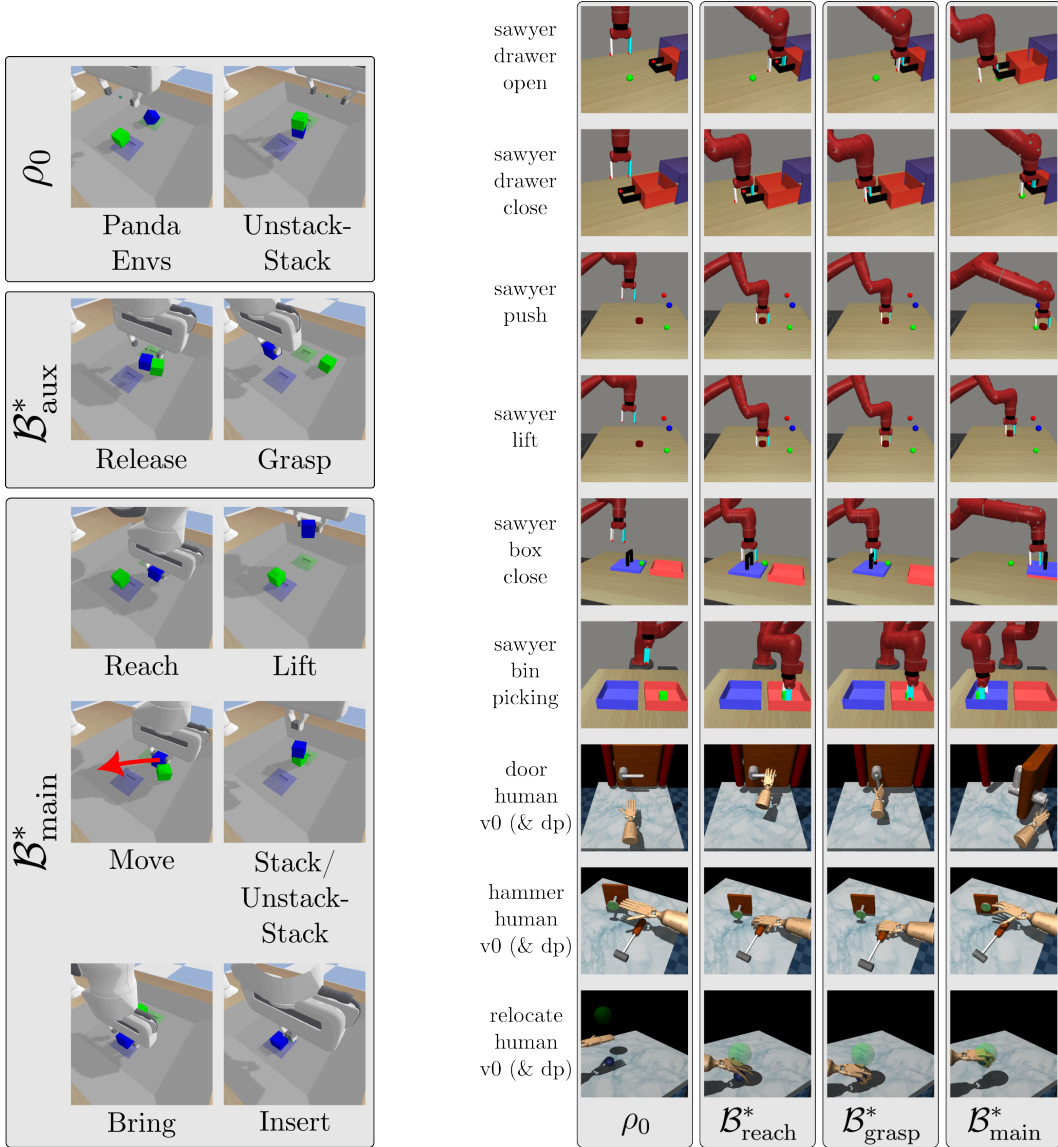
Algorithm 1 shows a summary of VPACE, built on LfGP [4] and SAC-X [31]. Table 1 shows a breakdown of some of the major differences between all of the algorithms studied in this work.

D.6 Additional Implementation Details

In this section, we list some specific implementation details of our algorithms. We only list parameters or choices that may be considered unique to this work, but a full list of all parameter choices can be found in our code. We also provide the VPACE pseudocode in Algorithm 1, with blue text only applying to learned discriminator-based reward functions (see Appendix A for various reward models).

Whenever possible, all algorithms and baselines use the same modifications. Table 2 also shows our choices for common off-policy RL hyperparameters as well as choices for those introduced by this work.

DAC reward function: for VPACE-DAC and VP-DAC, although there are many options for reward functions that map D to \hat{R} [45], following [4, 5, 17], we set the reward to $\hat{R}_{\mathcal{T}}(s) = \log(D_{\mathcal{T}}(s)) - \log(1 - D_{\mathcal{T}}(s))$.



(a) Panda ρ_0 and $\mathcal{B}_{\mathcal{T}}^*$ examples.

(b) Sawyer and Adroit ρ_0 and $\mathcal{B}_{\mathcal{T}}^*$ examples.

(c) Real Panda ρ_0 and $\mathcal{B}_{\mathcal{T}}^*$ examples.

Figure 9: Examples of samples from initial state distribution ρ_0 , auxiliary task buffers $\mathcal{B}_{\text{aux}}^*$, and main task buffers $\mathcal{B}_{\text{main}}^*$ for all environments and tasks used in this work. Auxiliary task data is reused between tasks in the Panda environment, since the observation space and action space are shared for all tasks, while only the task definitions themselves are reusable in the Panda and Adroit environments. Images are shown here for illustrative purposes, but all algorithms tested in this work use numerical state data.

Algorithm 1 Value-Penalized Auxiliary Control from Examples (VPACE)

Input: Example state buffers $\mathcal{B}_{\text{main}}^*, \mathcal{B}_1^*, \dots, \mathcal{B}_K^*$, scheduler period ξ , sample batch size N and N^* , and discount factor γ

Parameters: Intentions $\pi_{\mathcal{T}}$ with corresponding Q-functions $Q_{\mathcal{T}}$ (and optionally discriminators $D_{\mathcal{T}}$), and scheduler π_S (e.g. with Q-table Q_S)

```
1: Initialize replay buffer  $\mathcal{B}$ 
2: for  $t = 1, \dots$ , do
3:   # Interact with environment
4:   For every  $\xi$  steps, select intention  $\pi_{\mathcal{T}}$  using  $\pi_S$ 
5:   Select action  $a_t$  using  $\pi_{\mathcal{T}}$ 
6:   Execute action  $a_t$  and observe next state  $s'_t$ 
7:   Store transition  $\langle s_t, a_t, s'_t \rangle$  in  $\mathcal{B}$ 
8:
9:   # Optionally update discriminator  $D_{\mathcal{T}'}$  for each task  $\mathcal{T}'$ 
10:  Sample  $\{s_i\}_{i=1}^N \sim \mathcal{B}$ 
11:  for each task  $\mathcal{T}'$  do
12:    Sample  $\{s_i^*\}_{i=1}^{N^*} \sim \mathcal{B}_k^*$ 
13:    Update  $D_{\mathcal{T}'}$  following Eq. (3) using GAN + Gradient Penalty
14:  end for
15:
16:  # Update intentions  $\pi_{\mathcal{T}'}$  and Q-functions  $Q_{\mathcal{T}'}$  for each task  $\mathcal{T}'$ 
17:  Sample  $\{(s_i, a_i)\}_{i=1}^N \sim \mathcal{B}$ 
18:  for each task  $\mathcal{T}'$  do
19:    Sample  $\{s_i^*\}_{i=1}^{N^*} \sim \mathcal{B}_{\mathcal{T}'}$ 
20:    Sample  $a_i^* \sim \pi_{\mathcal{T}'}(s_i^*)$  for  $i = 1, \dots, N^*$ 
21:    Compute rewards  $\hat{R}_{\mathcal{T}'}(s_i)$  and  $\hat{R}_{\mathcal{T}'}(s_j^*)$  for  $i = 1, \dots, N$  and  $j = 1, \dots, N^*$ 
22:    # Compute value penalization terms, see Appendix D.6.1
23:    Compute  $Q_{\max}^{\pi_{\mathcal{T}'}} = \frac{1}{N^*} \sum_{j=1}^{N^*} Q(s_j^*, a_j^*)$ 
24:    Compute  $Q_{\min}^{\pi_{\mathcal{T}'}} = \min(\wedge_{i=1}^N \hat{R}_{\mathcal{T}'}(s_i), \wedge_{j=1}^{N^*} \hat{R}_{\mathcal{T}'}(s_j^*)) / (1 - \gamma)$ 
25:  end for
26:  Update  $\pi$  following Eq. (4)
27:  Update  $Q$  following Eq. (5) with value penalization Eq. (10)
28:
29:  # Optional Update learned scheduler  $\pi_S$ 
30:  if at the end of effective horizon then
31:    Compute main task return  $G_{\mathcal{T}_{\text{main}}}$  using reward estimate from  $D_{\text{main}}$ 
32:    Update  $\pi_S$  (e.g. update Q-table  $Q_S$  using EMA and recompute Boltzmann distribution)
33:  end if
34: end for
```

n -step returns and entropy in TD error: following results from [3], we also add n -step returns and remove the entropy bonus in the calculation of the TD error for all algorithms in all Sawyer and Adroit environments, finding a significant performance gain for doing so.

Absorbing states and terminal states: for all algorithms, we do not include absorbing states (introduced in [5]) or terminal markers (sometimes referred to as “done”), since we found that both of these additions cause major bootstrapping problems when environments only terminate on timeouts, and timeouts do not necessarily indicate failure. Previous work supports bootstrapping on terminal states when they are caused by non-failure timeouts [36].

SQIL labels for policy data: The original implementation of SQIL uses labels of 0 and 1 TD updates in Eq. (11) and Eq. (12), respectively. We found that changing the label for Eq. (11) from 0 to -1 improved performance.

<i>General</i>	
Total Interactions	Task-specific (see Appendix E)
Buffer Size	Same as total interactions
Buffer Warmup	5k
Initial Exploration	10k
Evaluations per task	50 (Panda), 30 (Sawyer/Adroit)
Evaluation frequency	25k (Panda), 10k (Sawyer/Adroit)
<i>Learning</i>	
γ	0.99
\mathcal{B} Batch Size	128
\mathcal{B}^* Batch Size	128
Q Update Freq.	1
Target Q Update Freq.	1
π Update Freq.	1
Polyak Averaging	1e-3
Q Learning Rate	3e-4
π Learning Rate	3e-4
D Learning Rate	3e-4
α Learning Rate	3e-4
Initial α	1e-2
Target Entropy	$-\dim(a)$
Max. Gradient Norm	10
Weight Decay (π, Q, D)	1e-2
D Gradient Penalty	10
Reward Scaling	0.1
SQIL Labels (Appendix D.6)	$(-1, 1)$
Expert Aug. Factor (Appendix D.6.3)	0.1
<i>Value Penalization (VP)</i>	
λ	10
$Q_{\max}^{\pi}, Q_{\min}^{\pi}$ num. filter points (Appendix D.6.1)	50
<i>Auxiliary Control (ACE) Scheduler (Appendix D.6.2)</i>	
Num. Periods	8 (Panda), 5 (Sawyer/Adroit)
Main Task Rate	0.5 (Panda), 0.0 (Sawyer/Adroit)
Handcraft Rate	0.5 (Panda), 1.0 (Sawyer/Adroit)

Table 2: Hyperparameters shared between all algorithms, unless otherwise noted.

Reward Scaling of .1: we use a reward scaling parameter of .1 for all implementations. Coupled with a discount rate $\gamma = 0.99$ (common for much work in RL), this sets the expected minimum and maximum Q values for SQIL to $\frac{-1}{1-\gamma} = -10$ and $\frac{1}{1-\gamma} = 10$.

No multitask weight sharing: intuitively, one may expect weight sharing to be helpful for multitask implementations. We found that it substantially hurt performance, so all of our multitask methods do not share weights between tasks or between actor and critic. However, the multitask discriminator in VPACE-DAC *does* have an initial set of shared weights due to its significantly poorer performance without this choice.

\mathcal{B}^* sampling for Q : in SQIL, DAC and RCE, we sample from both \mathcal{B} and \mathcal{B}^* for Q updates, but not for π updates (which only samples from \mathcal{B}). The original DAC implementation in [5] only samples \mathcal{B}^* for updating D , sampling only from \mathcal{B} for updating Q .

All other architecture details, including neural network parameters, are the same as [4], which our own implementations are built on top of. Our code is built on top of the code from [4], which was originally built using [46].

D.6.1 Maintaining $Q_{\max}^{\pi}, Q_{\min}^{\pi}$ Estimates for Value Penalization

Our approach to value penalization requires maintaining estimates for or choosing Q_{\max}^{π} and Q_{\min}^{π} . In both DAC and SQIL, the estimate of Q_{\max}^{π} comes from taking the mini-batch of data from \mathcal{B}^* , passing it through the Q function, taking the mean, and then using a median moving average filter to maintain an estimate. The “ $Q_{\max}^{\pi}, Q_{\min}^{\pi}$ num. filter points” value from Table 2 refers to the size of this filter. We chose 50 and used it for all of our experiments. We set Q_{\min}^{π} to

$$Q_{\min}^{\pi} = \frac{\text{rew. scale} \times \min(\hat{R}(s))}{1 - \gamma}, \quad (22)$$

where in SQIL, $\min(\hat{R}(s)) = \hat{R}(s)$ is set to 0 or -1, and in DAC, we maintain an estimate of the minimum learned reward $\min(\hat{R})$ using a median moving average filter with the same length as the one used for Q_{\max}^{π} .

D.6.2 Scheduler Choices

As noted in Section 4.1, our ACE algorithms use the same approach to scheduling from [4]. Specifically, we use a weighted random scheduler (WRS) combined a small set of handcrafted high-level trajectories. The WRS forms a prior categorical distribution over the set of tasks, with a higher probability mass $p\tau_{\text{main}}$ (Main Task Rate in Table 2) for the main task and $\frac{p\tau_{\text{main}}}{K}$ for all other tasks. Additionally, we choose whether to uniformly sample from a small set of handcrafted high-level trajectories, instead of from the WRS, at the *Handcraft Rate* from Table 2.

Our selections for handcrafted trajectories are quite simple, and reusable between main tasks within each environment. In the Panda tasks, there are eight scheduler periods per episode and four auxiliary tasks (*reach, grasp, lift, release*), and the handcrafted trajectory options are:

1. *reach, lift, main, release, reach, lift, main, release*
2. *lift, main, release, lift, main, release, lift, main*
3. *main, release, main, release, main, release, main, release*

In the Sawyer and Adroit environments, we actually found that the WRS was unnecessary to efficiently learn the main task, and simply used two handcrafted high-level trajectories. In these environments, there are five scheduler periods per episode and two auxiliary tasks (*reach, grasp*), and the handcrafted trajectory options are:

1. *reach, grasp, main, main, main*
2. *main, main, main, main, main*

D.6.3 Expert Data Augmentation

We added a method for augmenting our expert data to artificially increase dataset size. The approach is similar to other approaches that simply add Gaussian or uniform noise to data in the buffer [47, 48]. In our case, we go one step further than the approach from [48], and first calculate the per-dimension standard deviation of each observation in \mathcal{B}^* , scaling the Gaussian noise added to each dimension of each example based on the dimension’s standard deviation. For example, if a dimension in \mathcal{B}^* has zero standard deviation (e.g., in *Insert*, the pose of the blue block is always the same), it will have no noise added by our augmentation approach. The parameter “Expert Aug. Factor” from Table 2 controls the magnitude of this noise, after our per-dimension normalization scheme.

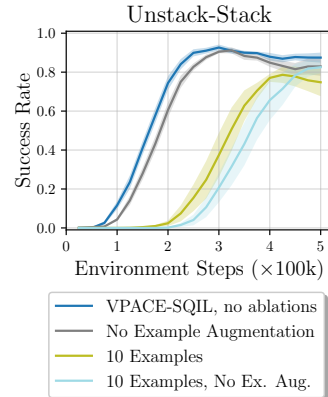


Figure 10: Additional results for the *Unstack-Stack* task from Fig. 11, either including or excluding the use of example augmentation described in Appendix D.6.3.

In Fig. 10, we show the results of excluding expert augmentation, where there is a clear, if slight, performance decrease when it is excluded, which is even more pronounced with a smaller B_T^* size. All methods and baselines from our own implementation use expert data augmentation.

D.6.4 Other Ablation Details

In our ablation experiments from Section 4.3, we included three baselines with full trajectory data, in addition to success examples. We added 200 (s, a) pairs from full expert trajectories to make datasets comparable to the datasets from [4], where they used 800 expert (s, a) pairs, but their environment was run at 20Hz instead of 5Hz, meaning they needed four times more data to have roughly the same total number of expert trajectories. We generated these trajectories using high-performing policies from our main experiments, since the raw trajectory data from [4] would not apply given that we changed the control rate from 20Hz to 5Hz.

D.6.5 Real Panda Implementation Details

While most of the design choices in Appendix D.6 apply to all environments tested, our real Panda environment had some small specific differences, mostly due to the complications of running reinforcement learning in the real world. We list the differences here, but for an exhaustive list, our open source code contains further details.

Maximum episode length: The maximum episode length for both `RealDrawer` and `RealDoor` is 1000 steps, or 200 seconds in real time. This was selected to reduce how often the environment had to be reset, which is time consuming. Running episodes for this long, and executing actions at 5 Hz, our environments complete 5000 environment steps in roughly 20 minutes. The extra time is due to the time to reset the environment after 1000 steps or after a collision. `VSPACE` took approximately 100 minutes to learn to complete `RealDrawer` consistently, and about 200 minutes to learn to complete the more difficult `RealDoor`.

Shorter initial exploration: To attempt to learn the tasks with fewer environment samples, we reduce buffer warmup to 500 steps, and initial random exploration to 1000 steps.

Frame stack: For training, we stacked two regular observations to avoid state aliasing.

Ending on success: We ended episodes early if they were determined to be successful at the main task only. Although this is not necessary for tasks to be learned (and this information was *not* provided to the learning algorithm), it gave us a way to evaluate training progress.

Extra gradient steps: To add efficiency during execution and training, we completed training steps during the gap in time between an action being executed and an observation being gathered. Instead of completing a single gradient step at this time, as is the case for standard SAC (and `VSPACE`), we completed four gradient steps, finding in simulated tasks that this gave a benefit to learning efficiency without harming performance. Previous work [4, 49] has found that increasing this update rate can reduce performance, but we hypothesize that our value penalization scheme helps mitigate this issue.

Collisions: If the robot is detected to have exceeded force or torque limits (20 N and 20 Nm in our case, respectively), the final observation prior to collision is recorded, and the environment is immediately reset. There are likely more efficient ways to handle such behaviour, but we did not investigate any in this work.

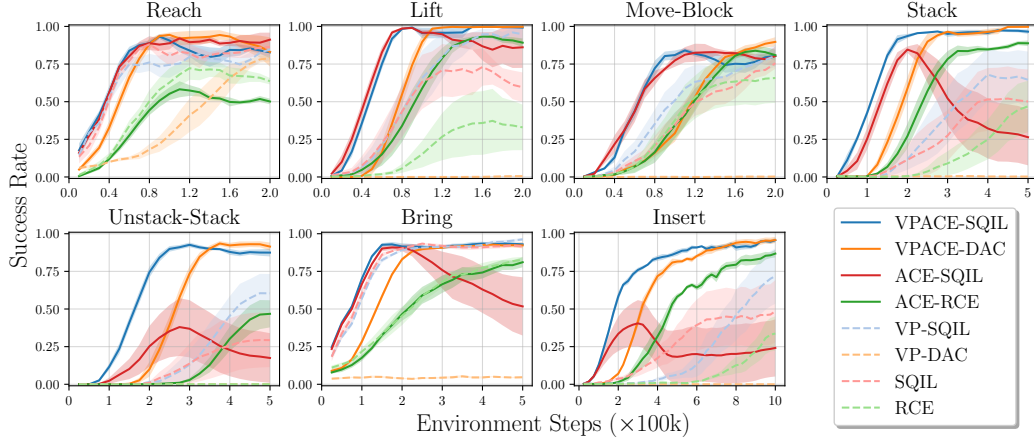


Figure 11: Performance results on simulated Panda tasks from [4, 32]. Performance on auxiliary tasks is not shown. Methods that leverage the multitask framework are shown with solid lines, and their single-task counterparts are shown with dashed lines. The shaded area corresponds to half standard deviation across five seeds. Both value-penalization and auxiliary task exploration are consistently beneficial for the most complicated tasks.

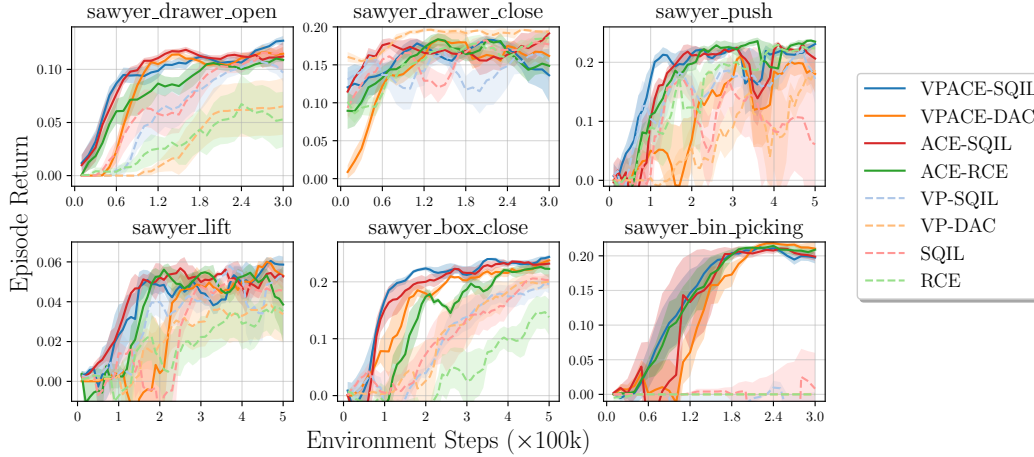


Figure 12: Performance results on the Sawyer tasks considered in [3] and introduced in [11]. For more complex tasks, the multitask methods learn with far fewer environment steps. These results are more stochastic than those from Fig. 11, but the same overall pattern emerges.

E Additional Performance Results

In this section, we expand upon our performance results from Section 4.2 and our Q-value calibration results from Section 4.4. We also show performance results for auxiliary tasks.

E.1 Expanded Main Task Performance Results

Fig. 11, Fig. 12, and Fig. 13 show expanded per-main-task results for our Panda (originally presented in [4, 32]), Sawyer (originally presented in [11, 3]), and Adroit Hand (originally presented in [37, 3]) tasks, respectively.

In the Panda tasks (Fig. 11), the hardest tasks (Stack, Unstack-Stack, and Insert) benefit the most from VPACE, but VPACE-SQIL is always the fastest and highest performing method. Notably, ACE-SQIL is always outperformed by both VPACE-SQIL and VPACE-DAC, and RCE is always outperformed by VP-SQIL. The benefits of value penalization are also clear, even in Bring, where ACE-SQIL initially learns the task, but starts to learn very poor Q estimates and have increasingly poorer and more unstable performance.

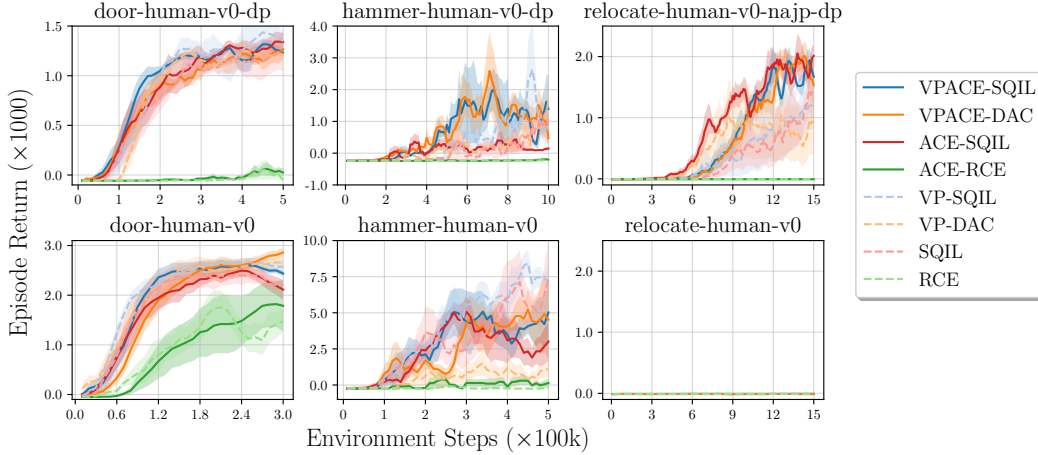


Figure 13: Performance results on the Adroit tasks considered in [3] and introduced in [37], along with modified versions of the environments that use delta-position based control. The episode return doesn’t fully represent the results for these environments, because the policies learned for the original tasks can be quite coarse and unrealistic (see Fig. 7). For the original environments, many baselines perform comparably, but for the dp versions, VPACE-SQIL, VP-SQIL, and VPACE-DAC are the most consistently high performing.

In the Sawyer tasks (Fig. 12), the benefit of VPACE is not as prominent, even if VPACE-SQIL is still the best performing method on average. The clearer pattern is the improvement from adding auxiliary task exploration, although the improvement is still lower, on average, than the improvement in the Panda tasks. Compared with the Panda tasks, these tasks do not have randomized initial conditions (apart from `sawyer_box_close`), and also generally require shorter movements to complete, so the benefits of VPACE are less pronounced.

In the Adroit hand tasks (Fig. 13), VPACE-SQIL, VPACE-DAC, and VP-SQIL are always among the highest performing methods. In particular, RCE and ACE-RCE are always outperformed by all other methods. As stated in Section 4.1 and further detailed in Appendix D.2, we also generated delta-position variants of the environments, which (i) generated, qualitatively, far more realistic policies (see Fig. 7), and (ii) allowed many methods to solve the `relocate` task.

E.2 Value Penalization Calibration Improvement – All Environments

This section expands on the value penalization calibration results from Section 4.4 for the Panda and Sawyer tasks Fig. 14 and for the Adroit hand tasks Fig. 15. Following the results shown for `Unstack-Stack`, the results for other difficult tasks also show clear violations of $y(s, a) \leq y(s^*, a^*)$, and tasks in which this rule is violated also tend to have poorer performance. The violations are more pronounced ACE-SQIL, which, as previously discussed, is likely because they generate far more diverse state distributions in \mathcal{B} . As shown for `Unstack-Stack` in Section 4.4, VP-SQIL and VPACE-SQIL never violate $y(s, a) \leq y(s^*, a^*)$. Intriguingly, although the rule is severely violated for many Adroit hand tasks, ACE-SQIL and SQIL still have reasonable performance in some cases. This shows that highly uncalibrated Q estimates can still, sometimes, lead to adequate performance. We hypothesize that this occurs because these tasks do not necessarily need $s_T \sim \mathcal{B}$ to match $s^* \sim \mathcal{B}_{\text{main}}^*$ to achieve high return, but we leave investigating this point to future work.

E.3 Auxiliary Task Performance Results

In our main text, we only presented performance results for main tasks, since our primary goal was to efficiently generate policies that performed well on a particular task. However, our scheduled auxiliary task approach inherently learns multiple auxiliary task policies $\pi_{\mathcal{T}_{\text{aux}}}$ in addition to the main task policy $\pi_{\mathcal{T}_{\text{main}}}$. While performance on these auxiliary task policies is not necessarily expected to be high throughout learning, observing auxiliary task performance can potentially provide useful

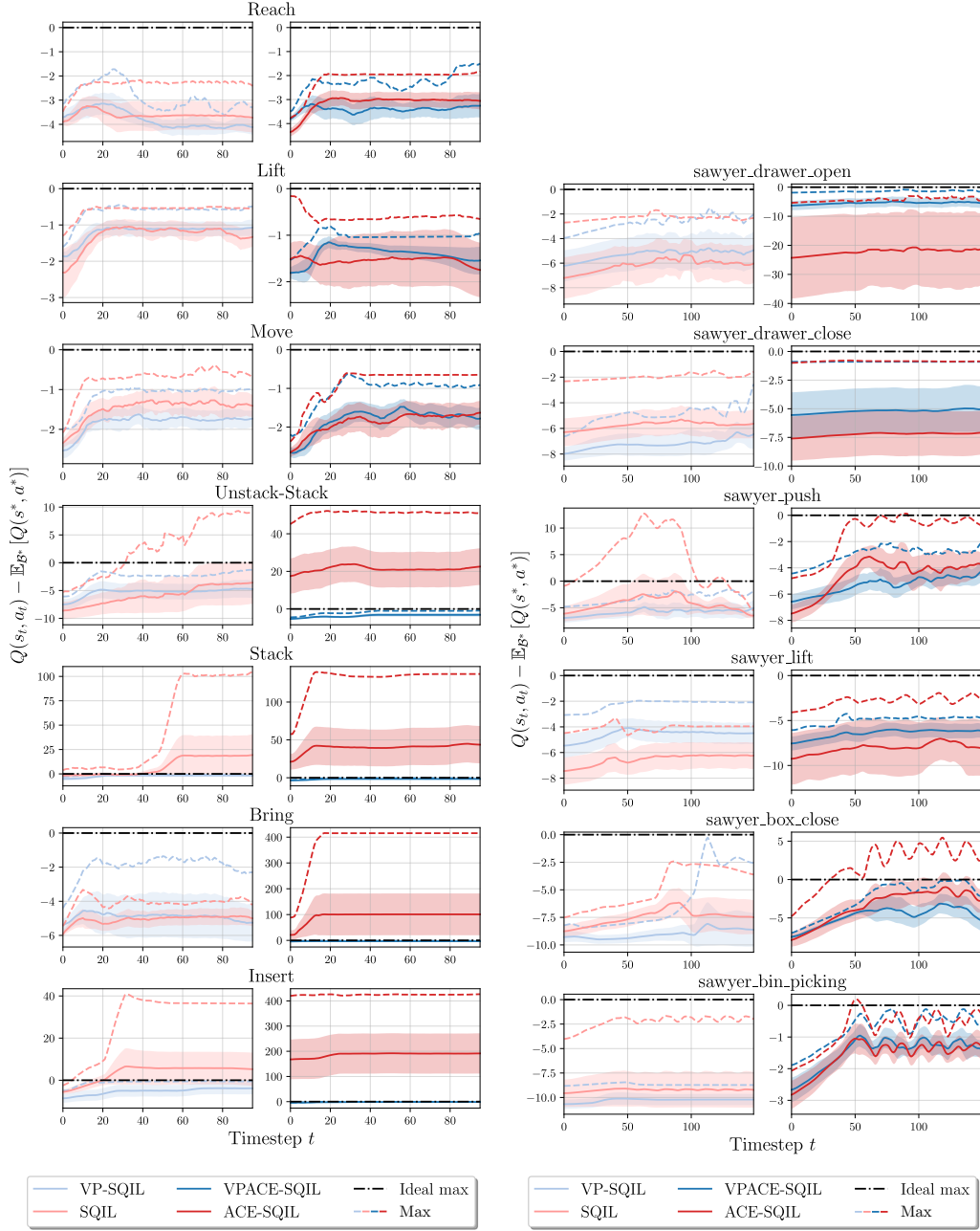


Figure 14: Additional results, from the Panda (left) and Sawyer (right) tasks, showing the difference between per-timestep Q values and the average Q values for data from $\mathcal{B}_{\text{main}}^*$. The most difficult tasks, with a larger variety of possible states, tend to have violations of the ideal maximum when value penalization is excluded, often exacerbated when ACE is used.

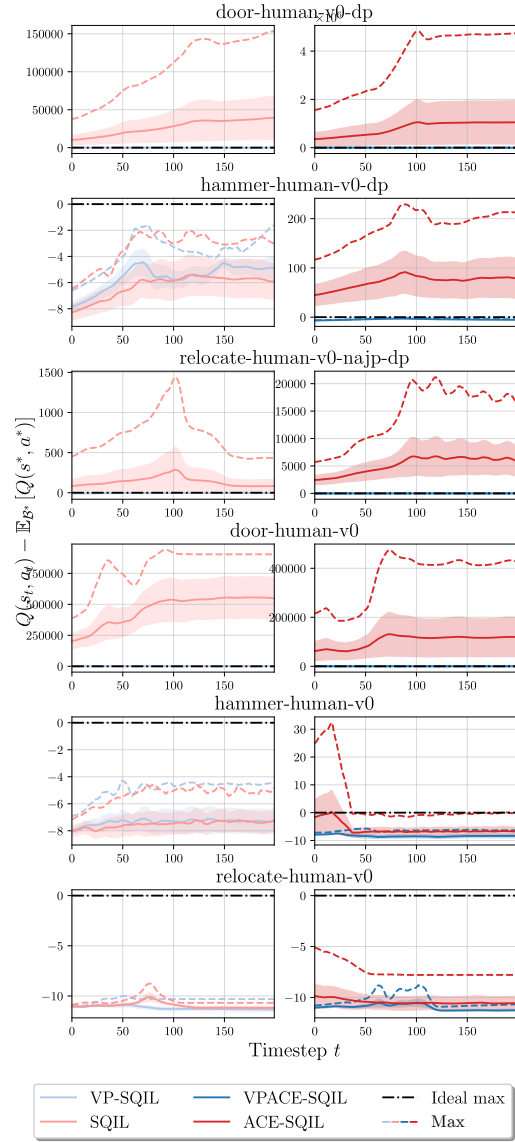


Figure 15: Additional results from the Adroit tasks showing the difference between per-timestep Q values and the average Q values for data from $\mathcal{B}_{\text{main}}^*$.

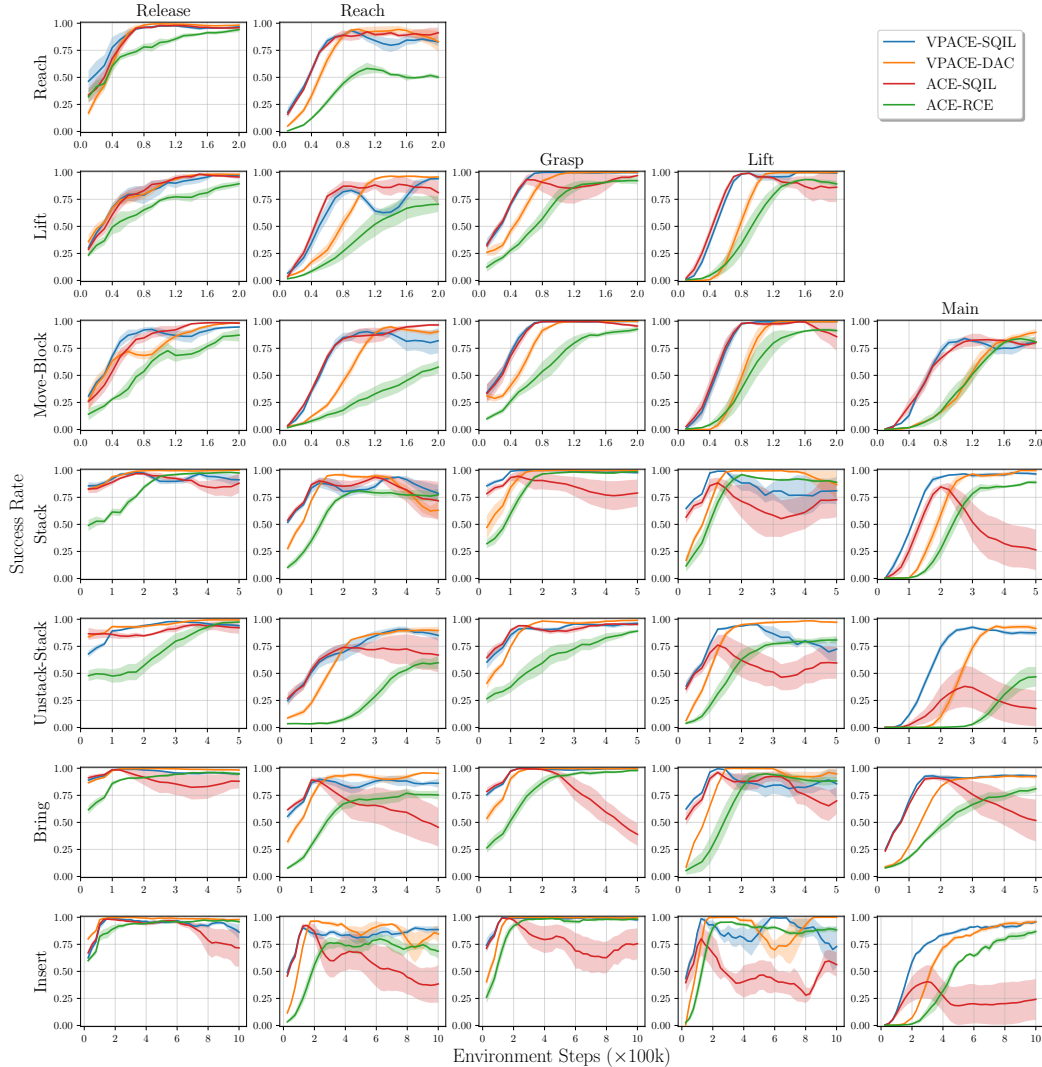


Figure 16: Auxiliary task performance for all of our methods that employ auxiliary control from examples. Main tasks are divided by row, and auxiliary tasks are divided by column, with the right-most column in each row showing main task performance. Performance on auxiliary tasks mostly follows performance on the main task, indicating that these auxiliary tasks may be useful for transfer learning to other main tasks.

insights, such as whether the auxiliary policies would be useful for transfer learning to learn a new main task.

We show all auxiliary task performance in for our Panda environments in Fig. 16. Auxiliary tasks tend to be learned slightly before the main task is learned, and otherwise auxiliary task performance generally follows performance on the main task (i.e. if the main task is learned slowly or poorly, auxiliary task performance will reflect this). The performance on the *Reach* auxiliary task is sometimes lower than on other, ostensibly more difficult tasks such as *Lift*, but this is likely because the success criteria for *Reach* is less forgiving than that for *Lift*.

We show auxiliary task performance for Sawyer and Adroit Hand environments in Fig. 17 and Fig. 18. Returns for auxiliary tasks are calculated based on reward functions originally taken from [3], in which a reaching reward is positive as an end-effector reaches closer to an object, and negative as it moves away, and grasp receives a similar bonus for moving or lifting the object of interest. In our ACE experiments for Sawyer and Adroit, we only use auxiliary tasks as part of a handcrafted high-level trajectory (see Appendix D.6.2), meaning that reach and grasp are only learned after a

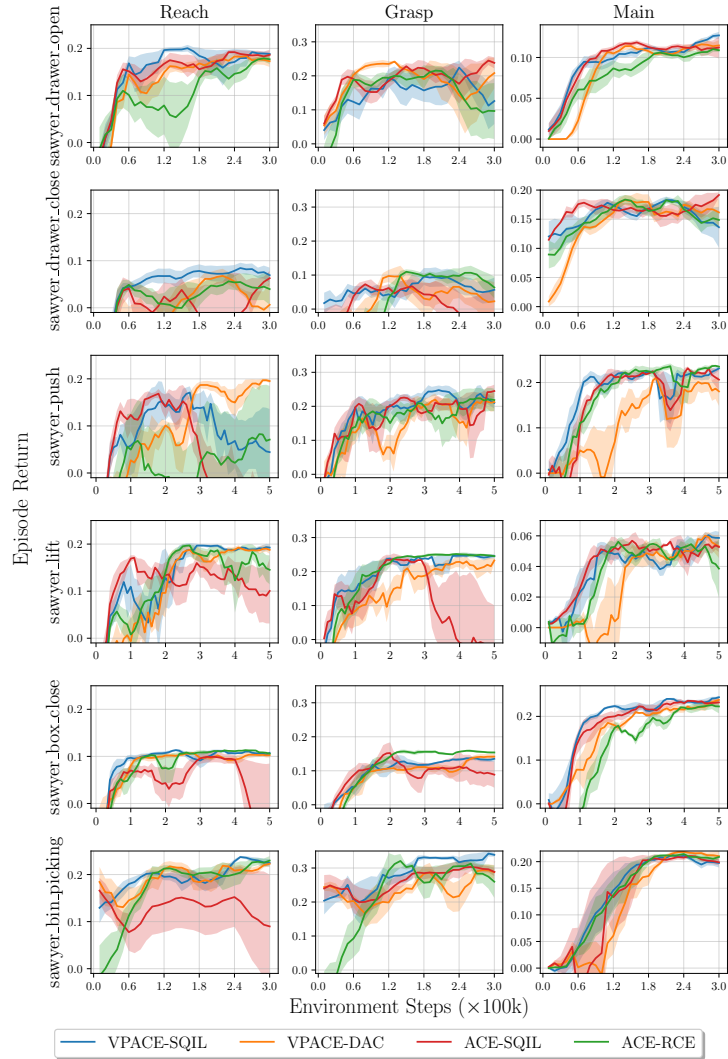


Figure 17: Sawyer auxiliary task performance. In the Sawyer tasks, auxiliary task varies but is often reasonable for methods with value penalization, and poorer when it is excluded.

reset, whereas during evaluation, the policy may have an opportunity to guide the end-effector to partially reach an object, then move away, with no learned strategy for recovery. We suspect that using a weighted random scheduler throughout learning may alleviate this issue, but we did not explore this in this work, since learning generally effective or reusable auxiliary tasks is beyond the scope of this work.

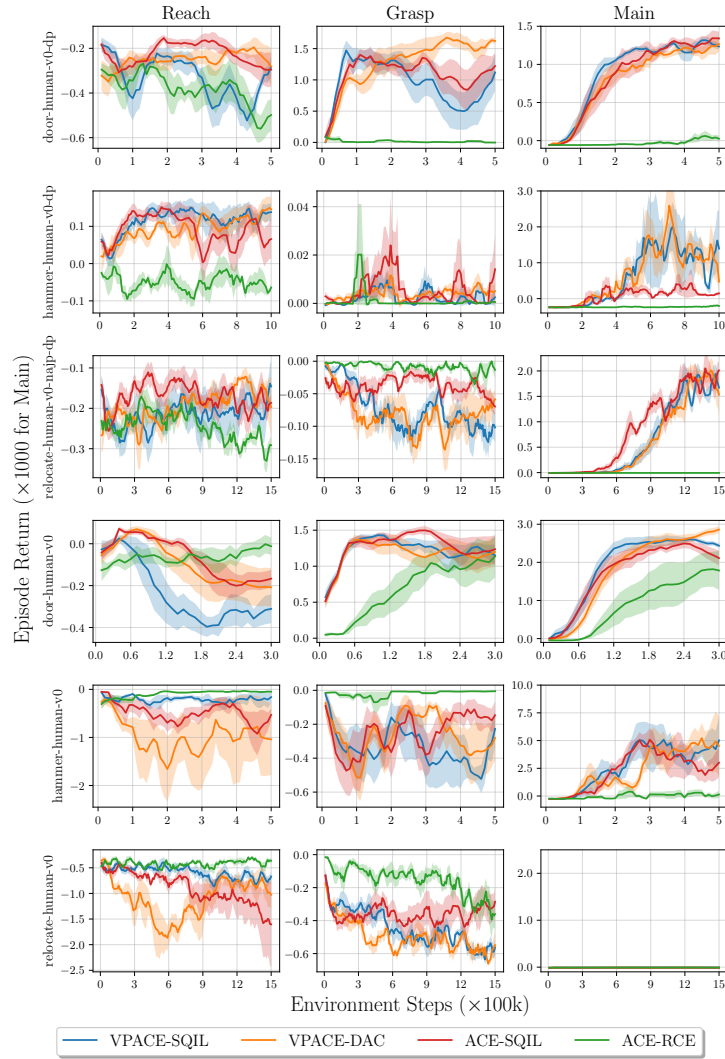


Figure 18: Adroit hand auxiliary task performance. Particularly in the hand environments, auxiliary task performance can be quite poor, which we expect is because we evaluate auxiliary tasks under different circumstances from how they are used during learning.

F Expanded Limitations

In this section, we expand on some of the limitations originally discussed in Section 5, where we previously skipped limitations that are inherent to reinforcement learning and to learning from guided play (LfGP, [4]), both of which are core parts of our approach.

Experimental limitation—Numerical state data only All of our tests are done with numerical data, instead of image-based data. Other work [31, 47] has shown that for some environments, image-based learning just results in slowing learning compared with numerical state data, and we assume that the same would be true for our method as well.

Assumption—Generating example success states is easier We claim that success example distributions are easier to generate than full trajectory expert data, and while we expect this to be true in almost all cases, there may still be tasks or environments where accomplishing this is not trivial. As well, similar to other imitation learning methods, knowing how much data is required to generate an effective policy is unknown, but adding a way to append to the existing success state distribution (e.g., [21]) would presumably help mitigate this.

Assumption/failure mode—Unimodal example distributions Although we do not explicitly claim that unimodal example state distributions are required for VPACE to work, all of our tested tasks have roughly unimodal example state distributions. It is not clear whether our method would gracefully extend to the multimodal case, and investigating this is an interesting direction for future work.

Experimental limitation—Some environment-specific hyperparameters While the vast majority of hyperparameters were transferable between all environments and algorithms, the scheduler period, the inclusion of n -step targets, and the use of entropy in TD updates, were different between environments to maximize performance. Scheduler periods will be different for all environments, but future work should further investigate why n -step targets and the inclusion of entropy in TD updates makes environment-specific differences.

F.1 VPACE and LfGP Limitations

VPACE shares the following limitations with LfGP [4].

Assumption—Existence of auxiliary task datasets VPACE and LfGP require the existence of auxiliary task example datasets $\mathcal{B}_{\text{aux}}^*$, in addition to a main task dataset $\mathcal{B}_{\text{main}}^*$. This places higher initial burden on the practitioner. In future, choosing environments where this data can be reused as much as possible will reduce this burden.

Assumption—Clear auxiliary task definitions VPACE and LfGP require a practitioner to manually define auxiliary tasks. We expect this to be comparatively easier than generating a similar dense reward function, since it does not require evaluating the relative contribution of individual auxiliary tasks. As well, all tasks studied in this work share task definitions, and the panda environment even shares task data itself, leading us to assume that these task definitions will extend to other manipulation tasks as well.

Assumption—Clear choices for handcrafted scheduler trajectories VPACE and LfGP use a combination of a weighted random scheduler with a handcrafted scheduler, randomly sampling from pre-defined trajectories of high level tasks. Ablett et al. [4] found that the handcrafted scheduler added little benefit compared with a weighted random scheduler, and further work should investigate this claim, or perhaps attempt to use a learned scheduler, as in [31].

F.2 Reinforcement Learning Limitations

Experimental limitation—Free environment exploration As is common in reinforcement learning methods, our method requires exploration of environments for a considerable amount of time (on the order of hours), which may be unacceptable for tasks with, e.g., delicate objects.